Cite as: M. Rigau *et al.*, *Science* 10.1126/science.aay5516 (2020).

Butyrophilin 2A1 is essential for phosphoantigen reactivity by γδ T cells

Marc Rigau[1,2,3], Simone Ostrouska[4,5], Thomas S. Fulford[1], Darryl N. Johnson[1,3], Katherine Woods[4,5,6], Zheng Ruan[1,3], Hamish E.G. McWilliam[1,7], Christopher Hudson[6], Candani Tutuka[4,5], Adam K. Wheatley[1,8], Stephen J. Kent[1,8], Jose A. Villadangos[1,7], Bhupinder Pal[4,5], Christian Kurts[2], Jason Simmonds[9], Matthias Pelzing[9], Andrew D. Nash[9], Andrew Hammet[9], Anne M. Verhagen[9], Gino Vairo[9], Eugene Maraskovsky[9], Con Panousis[9], Nicholas A. Gherardin[1], Jonathan Cebon[4,5,6], Dale I. Godfrey[1,3]*†, Andreas Behren[4,5,6,10]*†, Adam P. Uldrich[1,3]*†

[1]Department of Microbiology & Immunology at the Peter Doherty Institute for Infection and Immunity, The University of Melbourne, Parkville, Victoria 3010, Australia. [2]University of Bonn, Bonn, Germany. [3]Australian Research Council Centre of Excellence for Advanced Molecular Imaging at the University of Melbourne, Victoria 3010, Australia. [4]Olivia Newton-John Cancer Research Institute, Heidelberg, Victoria 3084, Australia. [5]School of Cancer Medicine, La Trobe University, Heidelberg, Victoria 3084, Australia. [6]Ludwig Institute for Cancer Research, Melbourne -Austin Branch Victoria 3084, Australia. [7]Department of Biochemistry and Molecular Biology at the Bio21 Molecular Science and Biotechnology Institute, The University of Melbourne, Parkville, Victoria 3010, Australia. [8]Australian Research Council Centre of Excellence for Convergent Bio-Nano Science and Technology at the University of Melbourne, Victoria 3010, Australia. [9]CSL Limited at the Bio21 Molecular Science and Biotechnology Institute, The University of Melbourne, Parkville, Victoria 3010, Australia. [10]Department of Medicine, The University of Melbourne, Melbourne, Victoria 3010, Australia.

*These authors contributed equally to this work.

†Corresponding author. E-mail: auldrich@unimelb.edu.au (A.P.U.); andreas.behren@onjcri.org.au (A.B.); godfrey@unimelb.edu.au (D.I.G.)

Gamma delta (γδ) T cells are essential to protective immunity. In humans, most γδ T cells express Vγ9Vδ2$^+$ T cell receptors (TCRs), which respond to phosphoantigens (pAg) produced by cellular pathogens and overexpressed by cancers. However, the molecular targets recognized by these γδTCRs are unknown. Here, we identify butyrophilin 2A1 (BTN2A1) as a key ligand that binds to the Vγ9$^+$ TCR γ-chain. BTN2A1 associates with another butyrophilin, BTN3A1, which act together to initiate responses to pAg. Furthermore, binding of a second ligand, possibly BTN3A1, to a separate TCR domain incorporating Vδ2 is also required. This unique mode of Ag-dependent T cell activation advances our understanding of diseases involving pAg recognition and creates opportunities for the development of γδ T cell-based immunotherapies.

αβ T cells recognize antigens (Ag) via T cell receptors (TCRs), encoded by *TRA* and *TRB* gene loci, which bind to Ag displayed by Ag-presenting molecules. This fundamental principle applies to αβ T cells that recognize peptide Ags presented by MHC molecules, NKT cells that recognize lipid Ags presented by CD1d, and mucosal-associated invariant T (MAIT) cells that recognize vitamin B metabolites presented by MR1 (*1*). γδ T cells are a unique lineage that express TCRs derived from separate variable (V), diversity (D), joining (J) and constant (C) *TRG* and *TRD* gene loci. Most circulating human γδ T cells express Vγ9Vδ2$^+$ TCRs that react to a distinct class of Ag, termed phosphoantigens (pAg) (*2*, *3*). pAgs are intermediates in the biosynthesis of isoprenoids, present in virtually all cellular organisms. Vertebrates produce isoprenoids via the mevalonate pathway, whereas microbes utilize the non-mevalonate pathway, and these pathways yield chemically distinct pAg intermediates (*4*). Vγ9Vδ2$^+$ T cells sense pAgs produced via either pathway, including isopentenyl pyrophosphate (IPP) from the mevalonate pathway and 4-hydroxy-3-methyl-but-2-enyl pyrophosphate (HMBPP) from the non-mevalonate pathway. However, these cells show roughly 1000-fold higher sensitivity for microbial HMBPP than vertebrate IPP pAgs (*5*). Thus, Vγ9Vδ2$^+$ T cells can respond to HMBPP derived from microbial infection, but also accumulated IPP in abnormal cells such as cancer cells. During bacterial and parasitic infections, pAg drives Vγ9Vδ2$^+$ T cells to produce cytokines and expand to represent ~10%–50% of peripheral blood mononuclear cells (PBMCs) (*6*, *7*). The important role that Vγ9Vδ2$^+$ T cells play in antibacterial immunity was demonstrated by human PBMC transfer into immune-deficient mice, which led to Vγ9Vδ2 T cell-dependent protection against bacterial infection (*8*). They can also kill diverse tumor cell lines in vitro in a pAg-dependent manner, and numerous clinical trials have examined their anticancer potential, with some encouraging results (*9*).

The molecular mechanisms governing pAg recognition by γδ T cells are unclear. Cell contact and Vγ9Vδ2 TCR expression are required, but classical Ag-presenting molecules such as MHC or MHC-like molecules are dispensable, suggesting a mechanism that is distinct from αβ T cell Ag recognition (*10*, *11*). Butyrophilin (BTN) surface protein BTN3A1 expression on Ag-presenting cells (APCs) plays a key role in pAg recognition (*12*), binding pAg via its intracellular B30.2 domain (*5*, *13*, *14*). Following pAg binding, BTN3A1 intracellular (*15*, *16*)

and extracellular (*17*) domains may undergo a conformational change that is important for γδTCR responses. This may be mimicked by an agonist anti-BTN3A1 mAb that stimulates Vγ9Vδ2$^+$ T cells without requiring exogenous pAg (*12*, *18*). However, a simplistic 1:1 interaction model between BTN3A1 and the γδTCR is unlikely because there is little evidence for a direct interaction between these molecules (*5*), and BTN3A1 transfection into rodent APCs fails to restore pAg-presenting capability, unless extra, undefined gene(s) on human chromosome 6 are included (*5*, *19*). Thus, other ligands in addition to BTN3A1 appear to be required for the γδ T cell response to pAg.

Here, we identify BTN2A1 as a direct ligand for the Vγ9Vδ2 TCR, and furthermore, we show that this ligand plays a critical role in pAg recognition by γδ T cells. BTN2A1 closely associates with BTN3A1 on the surface of APCs, and this complex can transmit pAg-mediated activation of Vγ9Vδ2$^+$ T cells. Accordingly, we propose a model whereby BTN2A1 acts in unison with BTN3A1 to license γδ T cell responses to pAg.

Results

BTN2A1 is a ligand for Vγ9$^+$ γδTCR

To identify candidate ligands for Vγ9Vδ2$^+$ γδ TCRs, we generated soluble Vγ9Vδ2$^+$ TCR tetramers derived from pAg-reactive γδ T cells (fig. S1) and used them to stain a diverse panel of human cell lines. This revealed clear staining of some lines including HEK-293T, but not others including the B cell line C1R (Fig. 1A). In particular, a melanoma cell line LM-MEL-62 was strongly stained (*20*) (Fig. 1A). Using a genome-wide knockdown screen (fig. S2), the most significant guide RNA (gRNA) responsible for Vγ9Vδ2$^+$ TCR-tetramer reactivity was *BTN2A1*, with a >13-fold enrichment compared to the controls. (Fig. 1A and fig. S2). BTN2A1 is a poorly characterized member of the butyrophilin family, found in humans but not mice. Like BTN3A1, it consists of two extracellular domains (IgV and IgC) and an intracellular B30.2 domain. Apart from one study suggesting it may interact with the C-type lectin receptor CD209 (DC-SIGN) in a glycosylation-dependent manner (*21*), BTN2A1 is generally considered an orphan receptor. To further investigate the significance of this finding, we confirmed a loss of reactivity to Vγ9Vδ2 TCR tetramers in two independent LM-MEL-62 *BTN2A1*-mutant lines (*BTN2A1*^{null1} and *BTN2A1*^{null2}), with similar results also from a distinct LM-MEL-75 *BTN2A1*-mutant cell line (Fig. 1C and fig. S3). This was independent of BTN3A1 expression, which was essentially unchanged between parental LM-MEL-62 and *BTN2A1*^{null} lines (Fig. 1C and fig. S3A). Additionally, Vγ9Vδ2 TCR tetramer reactivity of *BTN3A1*^{null} lines was comparable to parental lines (fig. S3B). Reintroduction of *BTN2A1* into either LM-MEL-62 *BTN2A1*^{null1} or *BTN2A1*^{null2} cells restored Vγ9Vδ2 TCR tetramer reactivity, whereas transfection with *BTN3A1* had no effect (Fig. 1D). Thus, BTN2A1 expression is essential for Vγ9Vδ2$^+$ TCR tetramer reactivity.

We next generated a panel of BTN2A1-reactive mAbs, which exhibited varying degrees of cross-reactivity to BTN2A2 (87% ectodomain homology) but not to BTN3A2 (45% ectodomain homology) (fig. S4A-C). These mAbs stained parental LM-MEL-62 but most failed to bind to LM-MEL-62 *BTN2A1*^{null} lines, confirming their reactivity to BTN2A1 (fig. S4D-E). Most of the anti-BTN2A1 mAbs fully or partially blocked Vγ9Vδ2 TCR tetramer staining on LM-MEL-62, LM-MEL-75, and 293T cells (Fig. 1E), suggesting that BTN2A1 is a ligand for the Vγ9Vδ2$^+$ γδTCR.

To explore whether BTN2A1 selectively binds to Vγ9Vδ2$^+$ γδ T cells, we produced fluorescent BTN2A1 ectodomain tetramers (fig. S5), which stained a subset of CD3$^+$ T cells within PBMCs, but no other cell type (Fig. 2A). The BTN2A1 tetramer$^+$ cells were γδTCR$^+$, but not αβTCR$^+$ (Fig. 2A). BTN2A1 tetramer labeled essentially all Vγ9$^+$Vδ2$^+$ and Vγ9$^+$Vδ1$^+$ γδ T cells, but no Vγ9$^-$Vδ1$^+$ γδ T cells, suggesting that the Vγ9 domain of the TCR γ-chain is associated with reactivity (Fig. 2B). Furthermore, Förster resonance energy transfer (FRET) between fluorescent BTN2A1 tetramer and anti-CD3ε mAb (*22*) indicated that BTN2A1 tetramer was binding within ~10 nm of the γδTCR (Fig. 2C). To directly assess whether BTN2A1 binds Vγ9$^+$ γδTCR, we performed surface plasmon resonance (SPR) to measure interactions between soluble BTN2A1 and γδTCR ectodomains. Consistent with the pattern of BTN2A1 tetramer reactivity amongst primary γδ T cells, soluble BTN2A1 bound TCR #6 (Vγ9Vδ2$^+$) with an affinity of K_D = 40 μM, similar to what is observed for classical αβ T cells (*23*). It also bound a "hybrid" γδTCR that co-expressed the TCR #6 γ-chain paired with an irrelevant Vδ1$^+$ γ-chain with comparable affinity (50 μM). However, BTN2A1 did not bind to a γδTCR comprising a Vγ5$^+$ γ-chain paired with the Vδ1$^+$ δ-chain (Fig. 2D). Lastly, we tested whether other butyrophilin family members could bind to Vγ9Vδ2 TCR. BTN2A2 exhibited only very weak binding, and BTN3A1+BTN3A2 and BTNL3+BTNL8 transfected cells did not bind Vγ9Vδ2 TCR tetramers (fig. S6). Thus, BTN2A1 is a ligand for Vγ9$^+$ γδTCR.

BTN2A1 is important for γδ T cell responses to pAg

We next determined if BTN2A1 is important in pAg-mediated γδ T cell responses. As expected, PBMCs cultured with the aminobisphosphonate compound zoledronate, which induces accumulation of the pAg IPP (*24*), resulted in Vδ2$^+$ but not Vδ1$^+$ γδ T cell induction of CD25, downregulation of surface CD3 (Fig. 3A), and production of IFN-γ and TNF (Fig. 3B). These indicators of TCR-dependent activation were significantly inhibited by anti-BTN2A1 mAb clone Hu34 and, to a lesser extent, by clones 259 and 267, compared to isotype control mAb-treated samples. Next, purified in vitro pre-

expanded Vγ9Vδ2$^+$ T cells were cultured with parental or *BTN2A1*^{null} LM-MEL-62 cells as APCs. Robust Vδ2$^+$ T cell responses to zoledronate, in terms of CD25 upregulation and CD3 downregulation, were observed in the presence of parental LM-MEL-62 APCs. However, both *BTN2A1*^{null1} and *BTN2A1*^{null2} APCs failed to promote γδ T cell activation above control cultures without APCs (Fig. 3C). Similarly, the proliferative expansion of Vδ2$^+$ γδ cells was diminished when *BTN2A1*^{null1} APCs were used (Fig. 3D). There was also γδ T cell-mediated, zoledronate-dependent, killing of parental LM-MEL-62 tumor cells, which was not observed with *BTN2A1*^{null1} cells, suggesting that BTN2A1 is important for Vγ9Vδ2$^+$ T cell cytotoxicity of tumor targets (Fig. 3D). Thus, BTN2A1 is important for γδ T cell responses to endogenous forms of pAg.

Vγ9Vδ2$^+$ γδ T cells can self-present high affinity foreign forms of pAg such as microbial HMBPP in the absence of APCs (*11*). BTN2A1 was also indispensable in this setting since purified in vitro pre-expanded Vδ2$^+$ T cells failed to upregulate CD25 and produce IFN-γ in the presence of neutralizing anti-BTN2A1 mAb (clones Hu34C, 227, 236, and 266) (Fig. 3E). Clone 267 was only a partial inhibitor of HMBPP-induced activation (Fig. 3E). Importantly, these mAbs did not inhibit anti-CD3 plus anti-CD28-mediated activation (Fig. 3E) nor did they block primary CD8$^+$ αβ T cell activation mediated by a mixture of viral peptides derived from cytomegalovirus, Epstein–Barr virus and influenza epitopes ("CEF" peptide, fig. S7). Thus, these BTN2A1 mAbs are specific antagonists of both self and foreign forms of pAg-driven T cell immunity. Taken together, BTN2A1 plays an important role in pAg-mediated Vγ9Vδ2$^+$ γδ T cell activation and resultant cytokine production, proliferation, and anti-tumor cytotoxicity by these cells.

BTN2A1 co-operates with BTN3A1 to elicit pAg responses by γδ T cells

We next determined if BTN2A1-dependent pAg responses are specifically mediated via γδTCR signaling. Following co-culture with either parental LM-MEL-75 or LM-MEL-62 APCs, J.RT3-T3.5 (Jurkat) T cells expressing the prototypical "G115" Vγ9Vδ2$^+$ TCR clonotype (*25*) upregulated CD69 in response to zoledronate. By contrast, *BTN2A1*^{null} and *BTN3A1*^{null} APCs largely failed to induce pAg reactivity (Fig. 4A). Untransduced (parental) Jurkat cells or those expressing an irrelevant γδTCR (clone 9C2 (*26*)) also failed to respond to pAg. Similar results were obtained using HMBPP and IPP (fig. S8A-C). Thus, BTN2A1 and BTN3A1 are both required to specifically mediate pAg responses in a Vγ9Vδ2$^+$ γδTCR-dependent manner.

Although BTN3A1 is essential for pAg-mediated responses, forced BTN3A1 overexpression fails to confer pAg-driven γδ T cell-stimulatory capacity to hamster and mouse APCs, indicating a requirement for other factors (*5*, *19*). We found that both hamster and mouse APCs transfected with *BTN2A1* and *BTN3A1* in combination, but not singly, were capable of pAg-dependent activation of γδ T cells (Fig. 4B and fig. S9A-B). Although another butyrophilin molecule, BTN3A2, was not necessary for this response, it moderately enhanced activation of γδ T cells when combined with BTN2A1 and BTN3A1, consistent with its potential role in increasing BTN3A1 activity (*27*). A modified *BTN2A1* construct with irrelevant transmembrane and intracellular domains derived from mouse paired immunoglobulin-like type 2 receptor beta, termed BTN2A1ΔB30, was also tested. This was still expressed on the cell surface and bound Vγ9Vδ2$^+$ TCR tetramer (fig. S9C), but it did not confer pAg-mediated activation (Fig. 4C). Thus, in addition to the role of its extracellular domain in binding Vγ9$^+$ γδTCR, the intracellular or transmembrane domain of BTN2A1 may also be important for pAg-mediated activation of Vγ9Vδ2$^+$ γδ T cells. This did not appear to be due to the intracellular B30.2 domain of BTN2A1 directly binding purified pAgs (HMBPP or IPP) because no clear interaction between these molecules was detected using isothermal titration calorimetry (fig. S10). This was in contrast to the clear interaction between the BTN3A1 B30.2 domain with pAg, as expected (*5*, *15*, *16*).

Lastly, we tested whether BTN2A1 and BTN3A1 induce pAg-mediated activation when expressed on the same cell (in cis) or on separate cells (in trans). BTN2A1$^+$ APCs mixed with either BTN3A1$^+$ APCs or BTN3A1$^+$BTN3A2$^+$ APCs, failed to elicit γδ T cell responses to pAg (Fig. 4D) suggesting that these molecules must be expressed on the same APC to mediate pAg-induced activation of γδ T cells.

BTN2A1 associates with BTN3A molecules on the cell surface

The requirement for BTN2A1 and BTN3A1 co-expression in cis raised the possibility that they associate with each other. Parental LM-MEL-75 cells stained with anti-BTN2A1 and anti-BTN3A1/3A2/3A3 ("BTN3A molecules") mAbs showed a similar staining pattern for BTN2A1 and BTN3A molecules on the cell surface (Fig. 5A-C). Pearson correlation coefficients indicated a significant overlap between the staining of BTN2A1 and BTN3A molecules, compared to the overlap of either with an irrelevant control (pan-HLA-A,B,C). Thus, BTN2A1 and BTN3A molecules appear to associate with one another on the plasma membrane (Fig. 5B). Furthermore, costaining of LM-MEL-75 cells with anti-BTN2A1 (clone 259) and anti-BTN3A (clone 103.2) resulted in a clear FRET signal (Fig. 5C), indicative of colocalization on the cell surface. Costaining with anti-BTN3A (clone 20.1) failed to cause FRET. Likewise, other anti-BTN2A1 clones (Hu34C and 267) resulted in only weak FRET. This may be because some mAb combinations yield spatially segregated donor and acceptor

fluorochromes beyond the 10-nm limit for FRET detection. Similar results were derived using mouse NIH-3T3 fibroblasts transfected with different combinations of BTN molecules (fig. S11). Interestingly, staining of BTN2A1ΔB30^{+}BTN3A1^{+} or BTN2A1ΔB30^{+}BTN3A2^{+} NIH-3T3 cells with anti-BTN2A1 and anti-BTN3A also resulted in FRET. The latter findings suggest that the association between these molecules is independent of the B30.2 domains, since BTN3A2 also lacks a B30.2 domain (fig. S11).

We next determined whether the intracellular domains of BTN2A1 and BTN3A1 are also associated by generating cyan fluorescent protein (CFP) or yellow fluorescent protein (YFP)-conjugated butyrophilin constructs (fig. S12). Co-transfection of mouse NIH-3T3 fibroblasts with BTN2A1^{CFP}+BTN3A1^{YFP}, or BTN2A1^{YFP}+BTN3A1^{CFP} resulted in clear FRET signals, similar to the positive controls that are known to associate (butyrophilin-like molecule 3 (BTNL3)^{CFP}+BTNL8^{YFP}) (*27*). Little to no FRET occurred in BTN3A1^{CFP}+BTNL8^{YFP} or BTNL3^{CFP}+BTN2A1^{YFP} or single-transfectant controls (Fig. 5D and fig. S13A). We also tested whether pAg modulated the FRET signal between BTN2A1 and BTN3A1 but did not detect any major changes (fig. S13B-C). However, anti-BTN2A1 mAb clones with antagonist activity (from Fig. 3D) all strongly disrupted their association (fig. S14). Thus, both the extracellular and intracellular domains of BTN2A1 and BTN3A1 are closely associated.

Vγ9Vδ2^{+} γδTCR recognizes at least two ligands

Given that BTN2A1 binds all Vγ9^{+} γδTCRs yet only Vγ9Vδ2^{+} T cells are pAg-reactive, we hypothesized that Vδ2 is also involved in this interaction. A corollary of this hypothesis could be that separate binding domains exist on the Vγ9Vδ2^{+} γδTCR, one responsible for binding BTN2A1, located within the germline-encoded region of Vγ9, and another that is also responsible for pAg reactivity, incorporating Vδ2 specificity. Mutations of Vγ9 residues Arg20, Glu70, and His85 (and to a lesser extent Glu22) to Ala all resulted in complete loss of BTN2A1 tetramer reactivity, whereas none of the Vδ2 mutations affected this. (Fig. 6A). The side chains of these Vγ9 residues were in close proximity to one another (Glu70-His85 distance 2.8 Å; His85-Arg20 distance 5.1 Å), and located on the outer faces of the B, D, and E strands, respectively, of the ABED antiparallel β-sheet of Vγ9. Together they formed a polar triad within the framework region of Vγ9 (Fig. 6B), consistent with BTN2A1 binding to the vast majority of Vγ9^{+} T cells (Fig. 2B). Thus, BTN2A1 appears to bind to the side of Vγ9, distal to the δ-chain and not in the vicinity of the complementarity-determining region (CDR) loops that are typically associated with Ag-recognition.

We next examined which residues were important for mediating functional responses to pAg. Jurkat cells transduced with γδTCR mutants expressed similar levels of CD3/γδTCR complex on their surface and responded equivalently to immobilized anti-CD3 mAb (fig. S15). Mutations to each of the BTN2A1-binding triad of γ-chain mutants abrogated pAg-mediated Jurkat cell activation (Fig. 6B). However, mutations to two additional residues, Arg51 of the Vδ2-encoded CDR2 loop, and Lys108 of the CDR3 loop of the TCR γ-chain, also abrogated pAg-mediated activation (Fig. 6C and (*10*)). These residues had no effect on BTN2A1 binding (Fig. 6B) and were located on the opposite side of the TCR to the putative BTN2A1 footprint (~30–40 Å separation). However, they were in close proximity to one another (~11 Å) (Fig. 6D), thereby potentially representing a separate binding interface necessary for pAg-mediated activation via the Vγ9Vδ2^{+} γδTCR, but not for BTN2A1 binding. This second binding interface explains the importance of: (i) the Vδ2^{+} TCR δ-chain through involvement of germline-encoded residues, and (ii) the invariant nature of the CDR3γ motif amongst pAg-reactive γδ T cells, via engagement of specific residues within this loop.

Finally, we tested agonist BTN3A1 mAb (clone 20.1)-mediated activation, which is thought to mimic pAg-mediated signaling by conformational modulation or cross-linking of BTN3A1 (*12*). Agonist BTN3A1 mAb-pulsed parental APCs induced Vγ9Vδ2 γδTCR^{+} Jurkat cell activation (Fig. 7), suggesting that BTN2A1 is critical for BTN3A1-mediated activation of γδ T cells. Furthermore, Jurkat cells expressing TCR γ-chain Ala mutants of the BTN2A1-binding residues His85, Arg20, and Glu70, as well as BTN2A1-independent mutants of Arg51 (δ-chain) and Lys108 (γ-chain), all failed to respond to parental APCs pulsed with agonist anti-BTN3A1 mAb (Fig. 7). Thus, an interaction between BTN2A1 and the Vγ9^{+} TCR γ-chain is essential, but not sufficient, for BTN3A1-driven γδ T cell responses. This fact may explain why, in earlier studies, the agonist anti-BTN3A1 mAb failed to induce activation of γδ T cells in co-cultures with mouse-derived APCs transfected with human BTN3A1 alone (*5*), because mice do not express BTN2A1.

Accordingly, these mutant studies indicate the existence of two separate interaction sites on Vγ9Vδ2^{+} γδTCRs necessary for pAg- and BTN3A1-mediated activation. One site on the side of the Vγ9 domain is essential for both BTN2A1 binding and for activation, whereas the other site, incorporating both the Vδ2-encoded CDR2 and γ-chain-encoded CDR3 loops, is required for pAg- and BTN3A1-mediated activation. Thus, Vγ9Vδ2^{+} T cells appear to be selectively activated by pAg though a distinct, dual-ligand interaction whereby BTN2A1 binds to the Vγ9 domain and another ligand, potentially BTN3A1, binds to a separate interface incorporating both the Vγ9 and Vδ2 domains.

Concluding remarks

Our findings support a model whereby BTN2A1 and BTN3A1 associate on the cell surface and are both required for pAg-

mediated γδ T cell activation. This model also suggests that after pAg binds BTN3A1 via its intracellular B30.2 domain, the BTN2A1–BTN3A1 complex engages the γδTCR via two distinct binding sites: BTN2A1 binds to Vγ9 framework regions, whereas another ligand—possibly BTN3A1—binds to the Vδ2-encoded CDR2 and γ-chain-encoded CDR3 loops on the opposite side of the TCR. This represents a distinct model of Ag sensing that is highly divergent from canonical MHC-Ag complex recognition by αβ T cells.

A previous study, using short hairpin RNA (shRNA) knockdown, found no apparent role for BTN2A1 in pAg presentation (*28*). However, as the knockdown efficiency was only 81% and BTN2A1 protein was not measured, residual BTN2A1 may have retained functionality. Until now, BTN2A1 has been poorly characterized, with only one earlier study identifying a glycosylation-dependent receptor, CD209 (*21*). We found that N-linked glycans were dispensable for BTN2A1 binding to the γδTCR (fig. S16), making it unlikely that CD209 plays a role in this interaction. Although little is known about the expression pattern of BTN2A1, RNA analysis predicts broad expression on immune cells. We confirmed that BTN2A1 is expressed on circulating B, T, and NK cells, monocytes, as well as Vγ9Vδ2$^+$ T cells (fig. S17), potentially explaining how γδ T cells can present pAg to themselves (*11*).

Recent studies revealed that human BTNL*3* and BTNL8 co-associate, and are stimulatory to human Vγ4$^+$ γδ T cells, with BTNL*3* interacting with a germline-encoded region of the γ-chain variable domain termed the HV4 loop (*29*, *30*). Likewise, mouse BTNL1 and BTNL*6* are linked and important for intestinal Vγ7$^+$ γδ T cell function and appear to bind to a similar region of the γδTCR (*29*, *30*). In contrast, the BTN2A1–Vγ9 binding interface appears to exhibit greater dependency on the outer face of the ABED β-sheet of the Vγ9 TCR than the HV4 loop, indicating that the BTN2A1-binding footprint on Vγ9 may be located further away from the CDR loops and closer to the Cγ domain. Given the tendency of butyrophilin molecules to dimerize (e.g., BTN3A1 can form stable V-shaped homodimers, and also heterodimers with BTN3A2 (*15*), and BTNL*3*–BTNL8 heterodimers (*30*)), it is possible that the association between BTN2A1 and BTN3A1 represents a direct interaction, although the molecular basis for this remains to be determined.

Compared to other Ag-presenting molecules (MHC and MHC-like molecules), the recognition of heteromeric butyrophilin complexes represents a fundamentally distinct class of immune recognition. It is not yet known how pAg alters this complex in order to induce antigenicity, but it may involve butyrophilin dimer or multimer remodeling, and/or conformational changes to BTN2A1 and BTN3A1. Other associated molecules such as ABCA1 (*31*) may be directly required, although based on our data these would need to be conserved across humans, mice, and hamsters.

In conclusion, this study significantly advances our understanding of how pAg are sensed by γδ T cells. In light of the mixed outcomes in numerous clinical trials that have utilized γδ T cells for anti-cancer therapy via pAg stimulation (*9*), it will be important to re-examine those data to determine if BTN2A1 expression holds prognostic and/or therapeutic value. Our findings also suggest BTN2A1 may represent a direct target for agonistic and/or antagonistic intervention in γδ T cell-mediated immunotherapy for infectious disease, cancer, and autoimmunity.

Methods

Human samples

Healthy donor blood derived human peripheral blood cells (PBMCs) were obtained from the Australian Red Cross Blood Service under ethics approval 17-08VIC-16 or 16-12VIC-03, with ethics approval from University of Melbourne Human Ethics Sub-Committee (1035100) or Olivia Newton John Cancer Research Institute (ONJCRI) Austin Health Human Research Ethics Committee (H2012-04446) and isolated via density gradient centrifugation (Ficoll-Paque PLUS GE Health care) and red blood cell lysis (ACK buffer, produced in-house). Established cell lines were routinely verified as *Mycoplasma*-negative using the MycoAlert test (Lonza).

Flow cytometry

Human cells were pelleted (400 × *g*), washed, and incubated at 4°C with PBS/2% fetal bovine serum (FBS) containing human Fc receptor block (Miltenyi Biotec). Mouse NIH-3T3 cells were incubated with anti-CD16/CD32 (clone 2.4G2, produced in-house). Cells were then incubated with 7-aminoactinomycin D (7-AAD, Sigma) or LIVE/DEAD® viability markers (ThermoFisher) plus antibodies (table S1). BTN2A1 and BTN3A were detected using monoclonal antibodies generated in-house (see below). Anti-BTN2A1 mAb or matched isotype control (clone BM4, produced in house) were conjugated to Alexa Fluor®-647 via amine coupling (ThermoFisher), and anti-BTN3A (clone 103.2) was conjugated to R-phycoerythrin (Prozyme) using sulfo-SMCC heterobifunctional crosslinker. In some experiments, unconjugated anti-BTN2A1 mAb were detected using goat anti-mouse polyclonal secondary antibody BV421 or PE (BD-Pharmingen), with a subsequent blocking step (5% normal mouse serum). Cells were also stained with tetrameric Vγ9Vδ2$^+$ γδTCR, BTN2A1, MR1–5-OP-RU, or mouse CD1d–α-GalCer ectodomains (produced in house, see below), or equivalent amounts of streptavidin conjugate alone (BD). Each reagent was titrated to determine the optimal dilution factor. All data were acquired on an LSRFortessa II, FACSCanto (BD), or CytoFLEX LX (Beckman Coulter), and analyzed with FACSDiva and FlowJo (BD) software. All samples were gated to exclude unstable events, doublets, and dead cells

using time, forward scatter area versus height, and viability dye parameters, respectively.

γδ T cell isolation and expansion

In some experiments γδ T cells were enriched by MACS using PE-Cy7-conjugated anti-γδTCR followed by anti-phycoerythrin-mediated magnetic bead purification (Miltenyi Biotec). After enrichment $CD3^+V\delta2^+$ γδ T cells were further purified by sorting using an Aria III (BD). Enriched γδ T cells were stimulated in vitro for 48 hours with plate-bound anti-CD3ε (OKT3, 10 μg/ml, Bio-X-Cell), soluble anti-CD28 (CD28.2, 1 μg/ml, BD Pharmingen), phytohemagglutinin (0.5 μg/ml, Sigma), IL-15 (50 ng/ml), and recombinant human IL-2 (100 U/ml, PeproTech), followed by maintenance with IL-2 and IL-15 for 14–21 days. Cells were cultured in complete medium consisting of a 50:50 (v/v) mixture of RPMI-1640 and AIM-V (Invitrogen) supplemented with 10% (v/v) FCS (JRH Biosciences), penicillin (100 U/ml), streptomycin (100 μg/ml), Glutamax (2 mM), sodium pyruvate (1 mM), nonessential amino acids (0.1 mM), and HEPES buffer (15 mM), pH 7.2–7.5 (all from Invitrogen Life Technologies), plus 50 μM 2-mercaptoethanol (Sigma-Aldrich).

Transfections

BTN2A1, *BTN2A2*, *BTN3A1*, *BTN3A2*, *BTNL3* and *BTNL8* (all isoform 1) were cloned into pMIG II mammalian expression vector (a gift from D. Vignali (Addgene plasmid # 52107) (*32*) and verified by Sanger sequencing. Mouse NIH-3T3, hamster CHO-K1, human LM-MEL-62 cells were plated out the day before and transfected using FuGene HD® or Viafect™ in OptiMEM according to manufacturer's instructions. After 48 hours (72 hours with LM-MEL-62 cells) to enable gene expression, cells were tested for GFP and gene expression and subsequently used in phenotyping or functional assays.

γδ T cell functional assays

Fresh PBMC (2×10^6) were cultured in 24-well plates ± zoledronate (4 μM, Sigma) and purified mAb against BTN2A1, BTN3A1, or isotype control IgG1κ (MOPC-21, BioLegend) (10 μg/ml). After 24 hours $CD3\varepsilon^+\gamma\delta TCR^+V\delta2^{+/-}$ γδ T cell activation was assessed by flow cytometry and cytokine production was determined by cytometric bead array according to manufacturer's instructions (BD). For the assays in fig. S7, PBMC were cultured in 24-well plates and blocked for 30 min with mAb against BTN2A1, BTN3A1, or isotype control (10 μg/ml). Cells were then stimulated for 18 hours with combinations of HMBPP (0.5 ng/ml, Sigma), zoledronate (4 μM, Sigma) and CEF (1 μg/ml, Miltenyi) in addition to IL-2 (25 U/ml, Miltenyi), and Golgiplug protein transport inhibitor (BD Biosciences). Cells were surface-stained and then fixed and permeabilized using Foxp3/Transcription Factor Staining Buffer Set (Invitrogen) according to the manufacturer's protocol followed by staining with anti-IFN-γ (Biolegend). For co-culture assays, purified and in vitro-expanded γδ T cells (5×10^5) were incubated in 96-well plates with APCs (3×10^5) for 24 hours ± zoledronate (4 μM), and γδ T cell activation was determined by flow cytometry as above. Alternatively (in Fig. 3c), 4×10^4 primary γδ T cells purified from PBMC donors using a γδ T cell magnetic bead isolation kit (Miltenyi) were cultured at a 2:1 ratio with either LM-MEL-62 WT or *BTN2A1*^{null1} APC in the presence of 1 μM zoledronate for 2 days. Non-adherent cells were subsequently washed and cultured in fresh plates without APC for an additional 7 days in media plus 100 U/ml IL-2. $V\delta2^+$ γδ T cells were then enumerated by flow cytometry.

FRET assays

For detection of FRET between BTN2A1 and BTN3A1 ectodomains, cells were stained with PE-conjugated anti-BTN3A1 (donor), and Alexa 647-conjugated BTN2A1 (acceptor). FRET was detected in a compensated yellow 670/30 channel. CFP (mTurquoise2, donor) and YFP (mVenus, acceptor) constructs containing either a long (used for BTN3A1 and BTNL3) or short (used for BTN2A1 and BTNL8) flexible N-terminal linker (fig. S12B) were synthesized (ThermoFisher) and cloned into the C terminus of butyrophilin constructs between an in-frame MfeI site that was introduced by site-directed mutagenesis, and a 3′ SalI site, which also removed the pMIG IRES-GFP motif. CFP was detected in a violet 450/50 channel, YFP using yellow 585/15, and FRET using a violet 530/30 channel from which CFP and YFP spillover had been removed by compensation. The frequency of cells identified as $FRET^+$ was examined on gated CFP^+YFP^+ NIH-3T3 cells for dual tranfectants, and either CFP^+ or YFP^+ for single transfectants.

Tumor viability assays

Tumor (10^4) cells were plated out in 96-well plates in RF-10. The next day, 2×10^4 γδ T cells were added with 100 U/ml IL-2 (Miltenyi) ± 1 μM zoledronate (Sigma). After a 1- or 3-day incubation, viability was assessed by an MTS assay, with absorbance measured at 490 nm on a SpectroStar Nano plate reader (BMG Labtech) and corrected for background and normalized against wells containing APCs alone at each time point.

Single-cell γδTCR sequencing

$CD3\varepsilon^+\gamma\delta TCR^+V\delta2^+$ γδ T cells derived from healthy donor PBMCs were individually sorted. The γδTCR was then amplified with primers listed in table S2. PCR amplicons were then cloned into pHL-sec containing either γ- or δ-chain ectodomains (fig. S1C) for expression.

Whole-genome CRISPR/Cas9 knockout screen

The CRISPR/Cas9 knockout screen was performed essentially

as described (*33*). Briefly, a pooled lentiviral human gRNA knockout library containing n=6 gRNA per gene (GeCKOv2, a gift from F. Zhang, Addgene #1000000048) was transformed into Endura ElectroCompetent cells (Lucigen) at >500X coverage and grown in 1 l liquid Luria Broth cultures for 16 hours at 37°C. Plasmid DNA was purified (PureLink gigaprep, ThermoFisher) and gRNA abundance in pre- and post-amplified libraries was validated by sequencing of PCR-amplified libraries (Illumina HiSeq, 60×10^6 reads per sample), with <0.2% gRNA dropout. Lentiviral particles were produced by transient transfection of HEK-293T cells with the gRNA library DNA plus packaging plasmids using FuGENE® (Promega), and culture supernatant was titrated on LM-MEL-62 cells to determine the viral titer using puromycin (1 μg/ml, ThermoFisher). Four biological replicates of LM-MEL-62 cells (2×10^8 each) were transduced with the lentiviral library at a multiplicity of infection of ~0.3. Transduced cells were then selected with puromycin for an additional 5 days, after which $V\gamma9V\delta2^+$ γδTCR tetramer #6^{lo} cells were sorted from half of each replicate (~6×10^7), and the remaining half was used as the unsorted control. The sorted cells were re-expanded for ~2 weeks and subsequently re-sorted. This was repeated an additional two times in order to adequately enrich for a clear $V\gamma9V\delta2^+$ γδTCR tetramer #6^{lo} population of LM-MEL-62 cells (fig. S2A). Genomic DNA was then extracted as previously described (*34*), including an additional phenol–chloroform purification step. gRNA from ~6×10^7 unsorted and ~3×10^7 sorted cells was amplified from genomic DNA using PCR (33 cycles) with *Pfu*-based DNA polymerase (Herculase II Fusion, Agilent Technologies) and one-step primers containing index and adaptor sequences (IDT Ultramer oligos) as previously described (*33*). Amplicons were gel-extracted following electrophoresis (Wizard® SV Gel Clean-Up System, Promega), quantified with PicoGreen® (ThermoFisher) and sequenced using a NovaSeq (Illumina). Sample data were demultiplexed using a combination of the forward primer stagger motifs and the reverse 8-mer barcodes using Cutadapt (*35*) and analyzed using the EdgeR software package in R studio (*36*). Guides were enumerated using the *processAmplicons* function, allowing for a single base pair mismatch or shifted guide position. Guides with less than 0.5 counts/10^6 in at least five samples were excluded from the analysis. After dispersion estimation, differential gRNA expression between unsorted and sorted samples was determined using the *exactTest* function, where a false discovery rate (FDR) of <0.05 was considered statistically significant. The raw count files and analysis script are available in database S1.

Production of soluble proteins

Soluble human γδTCRs, butyrophilin 2A1 and mouse CD1d ectodomains were expressed by transient transfection of mammalian Expi293F or GNTI-defective HEK-293S cells using ExpiFectamine or PEI, respectively, with pHL-sec vector DNA encoding constructs with C-terminal biotin ligase (AviTag) and His_6 tags (*37*). MR1-5-OP-RU tetramer was produced as previously described (*38*). Protein was purified from culture supernatant using immobilized metal affinity chromatography (IMAC) and gel filtration, and enzymatically biotinylated using BirA (produced in-house). Proteins were re-purified by size exclusion chromatography and stored at −80°C. Biotinylated proteins were tetramerized with streptavidin-PE (BD) at a 4:1 molar ratio. DNA constructs encoding butyrophilin B30.2 intracellular domains with C-terminal His_6 tags were synthesized de novo (ThermoFisher) and cloned into pET-30 bacterial expression vectors. BL21 DE3 (pLysS) *E. coli* were used for overnight expressions at 30°C following induction with IPTG (1 mM). Cell pellets were washed and lysed using a sonicator in PBS/1 mM DTT and B30.2 proteins were purified from clarified lysate using IMAC and gel filtration.

Generation of anti-BTN2A1 mAb

A human antibody phage display library was used to screen for antibody clones with specificity for BTN2A1. Screening consisted of three rounds of selection for binding to 50 nM recombinant soluble C-terminally His-tagged BTN2A1 ectodomain immobilized on streptavidin-coated paramagnetic beads (Dynal), with pre-adsorption of non-specific binders on an unrelated control His-tagged protein also immobilized on streptavidin-coated beads. After extensive washing, bound phage were eluted and amplified overnight by infection of exponentially growing bacterial cultures (TG1; Stratagene). Purified phage were then used for a subsequent round of panning. After three rounds, bound phage were eluted and 190 clones were randomly picked and tested by ELISA for binding to BTN2A1 immobilized in a microplate. Sequencing of positive clones revealed a total of 52 individual antibody clones, of which 45 were then sub-cloned into a mammalian expression vector for expression in Expi293F cells (ThermoFisher) and purification on MabSelect SuRe resin (GE Lifesciences) as full-length IgG molecules which comprised a human IgG4 Fab region and murine IgG2a Fc region. Isotype control clone BM4 contained the same Fc region, except for a mouse Fab region with irrelevant specificity.

Production of anti-BTN3A antibodies

DNA constructs encoding anti-BTN3A antibody variable domains (clones 20.1 and 103.2) were synthesized (ThermoFisher) and cloned into mammalian expression vectors containing a mouse IGHV signal peptide and IgG1 constant regions. Antibodies were expressed in Expi293F cells as above and purified using Protein G column chromatography (GE), followed by buffer-exchange into PBS.

Enzyme-linked immunosorbent assay

Purified recombinant proteins (0.2–20 μg/ml) were immobilized in microplate wells in PBS buffer overnight at 4°C. Non-specific binding was then blocked by incubation in PBS containing 0.05% tween 20 plus 5% skim milk powder or 0.5% (w/v) bovine serum albumin (BSA). The wells were then incubated for 60 min at room temperature in the presence of antibodies at 2-5 μg/ml in PBS/0.05% Tween 20/2% skim milk powder or 0.5% BSA, followed by washing in PBS/0.05% Tween 20. Plates were then incubated with HRP-labeled sheep anti-mouse IgG secondary antibody (Chemicon), or goat anti-mouse IgG secondary antibody (Millipore) followed by detection using 3,3′,5,5′-tetramethylbenzidine substrate (Sigma) and absorbance was measured at 450 nm using a plate reader.

Generation of CRISPR/Cas9-mediated knockout cell lines

For BTN2A1 knockout lines two gRNAs (*BTN2A1*^{null1}: 5′-TCACAAAGGTGGTTCTTCCT-3′ and *BTN2A1*^{null2}: 5′-CAATAGATGCATACGGCAAT-3′) were cloned into GeneArt® CRISPR Nuclease Vector Kit (Life Technologies) according to the manufacturer's protocol and sequence-verified by Sanger sequencing. Cells were transfected using Lipofectamine 2000 and sorted after 48 hours based on orange fluorescent protein expression. Cells were cultured and stained with anti-BTN2A1 (clone Hu34C) and the negative fraction sorted. For *BTN3A1*-knockout lines, a *BTN3A1* CRISPR/Cas9 KO Plasmid kit (Santa Cruz Biotechnology) containing three specific gRNA sequences was used (5′-GGCACTTACGAGATGCATAC-3′, 5′-GAGAGACATTCAGCCTATAA-3′, 5′-ACCATCAGAAGTTCCCTCCT-3′). Cells were transfected using Lipofectamine 3000 (ThermoFisher) and sorted after 48 hours based on green fluorescent protein. Sorted cells were cultured and stained with anti-BTN3A1 (clone 103.2) and negative fraction sorted and cultured.

Jurkat assays

LM-MEL-62 or LM-MEL-75 APCs at 2.5 × 10^4 cells/well in a 96-well plate were incubated overnight. Then 2 × 10^4 G115 mutant γδTCR-expressing J.RT3-T3.5 (ATCC® TIB-153) Jurkat cells ± zoledronate, HMBPP or IPP were added for 20 hours. CD69 expression was then measured by flow cytometry on GFP$^+$ Jurkat cells. A panel of 19 single-residue alanine (Ala) mutants, each within in the Vγ9 or Vδ2 domains of the Vγ9Vδ2$^+$ G115 TCR were generated by site-directed mutagenesis using the primers listed in table S2). Primers (IDT) were phosphorylated (PNK, NEB) followed by 25 cycles of PCR using KAPA HiFi master mix (KAPA Biosystems) using WT G115 in pMIG as template, and PCR product was digested with DpnI (NEB) and ligated with T4 DNA ligase (NEB). Construct sequences were then verified by Sanger sequencing prior to transfections. To examine the capacity of G115 TCR mutants to bind to BTN2A1 tetramer, HEK-293T cells were transfected with individual γ-chain or δ-chain mutants, plus the corresponding WT δ- or γ- chain, respectively, as well as a pMIG construct encoding 2A-linked human CD3γδεζ, at a 1:3 ratio with FuGENE® HD (Promega) in OptiMEM (Gibco, ThermoFisher). 48 hours after transfection, HEK-293T cells were resuspended by pipetting, and stained for CD3ε expression and PE-labeled BTN2A1 tetramer or control PE-conjugated streptavidin. The median fluorescence intensity (MFI) of BTN2A1 tetramer interacting with mutant G115 TCRs was examined on gated CD3$^+$GFP$^+$ HEK-293T cells by flow cytometry.

The capacity of G115 mutants to respond to pAg stimulation was assessed by transducing J.RT3-T3.5 Jurkat cells with G115 mutant TCRs. HEK-293T cells were transfected with each particular γ-chain or δ-chain mutant, plus the corresponding wild-type δ- or γ-chain, respectively, along with human CD3, pVSV(-G), and pEQ-Pam3(-E), and mixed at a 1:3 ratio with FuGENE® HD in OptiMEM. After 24 hours, viral supernatants were collected and filtered through a 0.45-μm CA syringe filter, then incubated with JRT3-T3.5 Jurkat cells for 12 hours. This process was repeated twice a day for 4 days. CD3$^+$GFP$^+$ Jurkat cells were purified by FACS (BD FACSAria III) and examined for their capacity to respond to pAg presented by wild-type LM-MEL-75 APCs as described above.

To measure G115 γδTCR-expressing Jurkat cell reactivity to anti-BTN3A1 (clone 20.1) mAb, 2.5 × 10^4 LM-MEL-75 APC cells were pre-incubated with functional grade 20.1 (10 μg/ml, Biolegend), or matched isotype control for 30 min at room temperature and later plated in a flat-bottom 96-well plate. Once the APCs had adhered, 2.5 × 10^4 Jurkat cells were added making a final antibody concentration of 5 μg/ml. After 24 hours of co-culture, cell-surface CD69 expression by CD3$^+$GFP$^+$ Jurkat cells was determined by flow cytometry.

Surface plasmon resonance

SPR experiments were conducted at 25°C on a Biacore T200 instrument (GE Healthcare) using 10 mM HEPES-HCl (pH 7.4), 150 mM NaCl, 3 mM EDTA, and 0.05% Tween 20 buffer. γδTCR ectodomains were directly immobilized to 260 resonance units (RU) on a Biacore sensor chip SA pre-immobilized with streptavidin. Soluble butyrophilins were serially diluted (200–3.1 μM) and simultaneously injected over test and control surfaces at a rate of 30 μl/min. After subtraction of data from the control flow cell (streptavidin alone) and blank injections, interactions were analyzed using Biacore T200 evaluation software (GE Healthcare) and Prism version 8 (GraphPad), and equilibrium dissociation constants (K_D) were derived at equilibrium.

Isothermal titration calorimetry

ITC experiments were conducted on a MicroCal ITC200 instrument (GE Healthcare) at 25°C. BTN2A1 or BTN3A1 B30.2 domains were buffer exchanged into PBS, and adjusted to a final concentration of 100 μM. HMBPP (Cayman Chemical) and IPP were adjusted to final concentrations of 1.9 mM and 2 mM, respectively, and serially injected into the cell in 2-μl increments, following an initial 0.4-μl injection that was discarded from the analysis. Data were analyzed with Microcal Origin software.

Confocal microscopy

LM-MEL-75 WT, *BTN2A1*^{null}, *BTN3A1*^{null} cells were cultured overnight in RPMI-1640 (Thermo-Fisher) supplemented with 10% (v/v) FCS (JRH Biosciences), penicillin (100 U/ml), streptomycin (100 μg/ml), Glutamax (2 mM), sodium pyruvate (1 mM), nonessential amino acids (0.1 mM), and HEPES buffer (15 mM), pH 7.2–7.5 (all from Invitrogen Life Technologies), plus 50 μM 2-mercaptoethanol (Sigma-Aldrich) and allowed to adhere to chamber well slides (Lab-Tek, Thermo-Fisher). The following day, cells were washed and incubated with human Fc receptor block (Miltenyi Biotec) diluted with Opti-MEM (Thermo-Fisher) on ice for 20 min. Cells were washed and stained with anti-BTN2A1-AF647 (clone 259), anti-BTN3A-PE (clone 103.2), and anti-pan-HLA class I-AF488 (clone W6/32, BioLegend) diluted in Opti-MEM on ice for 20 min. Cells were fixed with 1% paraformaldehyde (Electron Microscopy Sciences) in PBS for 20 min then mounted with ProLong Gold AntiFade (Thermo-Fisher) and covered with a #1 coverslip (Menzel-Gläser) overnight. Each reagent was titrated to determine the optimal dilution factor. Z-stack, single tile images with 76.9 nm lateral and 400 nm axial voxel size and 1024 × 1024 voxel density were acquired on a LSM780 laser scanning confocal microscope with an inverted 20X (0.8NA) objective, PMT detectors, and Zen software (Zeiss). Fluorochromes were excited with 488-, 561-, and 633-nm laser lines. Images were deconvoluted with Huygens Professional (Scientific Volume Imaging) and analyzed with Imaris (Oxford Instruments) software. Regions of interest defining the imaged cells were made based on the brightfield channel and the Imaris Coloc module was used to calculate Pearson correlation coefficients of voxels with intensity thresholds set for each analyzed channel based on negative controls for each stain.

Immunoblotting

Cells were washed in PBS and lysed in Pierce RIPA buffer (Thermofisher) in the presence of complete protease inhibitor cocktail (Roche). Protein quantification in cell lysates was performed using Pierce BCA protein assay kit (Thermofisher). Samples were run on NuPAGE 4%–12% Bis-Tris protein gels (Invitrogen Life Technologies), and proteins were resolved by immunoblotting using the iBlot system (Invitrogen Life Technologies). Primary antibodies anti-BTN2A1 (0.2 μg/ml, Sigma Prestige) and GAPDH (0.04 μg/ml, Cell Signaling Technology) were detected with IRDye® 680RD goat anti-rabbit IgG secondary antibody (0.1 μg/ml, Licor). PVDF membrane was scanned using an Odyssey scanner.

Statistical analyses

For comparison of two independent groups, a nonparametric Mann–Whitney *U* test was used. For the comparison of more than two independent groups a Kruskal–Wallis test with a Dunn's post-test was used. For comparison of two paired groups, a Wilcoxon test was used. For comparison of more than two paired groups that were normally distributed (determined by a Kolmogorov–Smirnov test), a repeated-measures ANOVA and Dunnett's multiple comparison test was performed with individual variances computed for each comparison; otherwise, a Friedman test with a Dunn's post-test was used. All p-values less than 0.05 were considered statistically significant.

REFERENCES AND NOTES

1. J. Rossjohn, S. Gras, J. J. Miles, S. J. Turner, D. I. Godfrey, J. McCluskey, T cell antigen receptor recognition of antigen-presenting molecules. *Annu. Rev. Immunol.* **33**, 169–200 (2015). doi:10.1146/annurev-immunol-032414-112334 Medline
2. P. Constant, F. Davodeau, M. A. Peyrat, Y. Poquet, G. Puzo, M. Bonneville, J. J. Fournié, Stimulation of human gamma delta T cells by nonpeptidic mycobacterial ligands. *Science* **264**, 267–270 (1994). doi:10.1126/science.8146660 Medline
3. Y. Tanaka, C. T. Morita, Y. Tanaka, E. Nieves, M. B. Brenner, B. R. Bloom, Natural and synthetic non-peptide antigens recognized by human gamma delta T cells. *Nature* **375**, 155–158 (1995). doi:10.1038/375155a0 Medline
4. L. Zhao, W. C. Chang, Y. Xiao, H. W. Liu, P. Liu, Methylerythritol phosphate pathway of isoprenoid biosynthesis. *Annu. Rev. Biochem.* **82**, 497–530 (2013). doi:10.1146/annurev-biochem-052010-100934 Medline
5. A. Sandstrom, C.-M. Peigné, A. Léger, J. E. Crooks, F. Konczak, M.-C. Gesnel, R. Breathnach, M. Bonneville, E. Scotet, E. J. Adams, The intracellular B30.2 domain of butyrophilin 3A1 binds phosphoantigens to mediate activation of human $V_\gamma9V\delta2$ T cells. *Immunity* **40**, 490–500 (2014). doi:10.1016/j.immuni.2014.03.003 Medline
6. Y. L. Wu, Y.-P. Ding, Y. Tanaka, L.-W. Shen, C.-H. Wei, N. Minato, W. Zhang, γδ T cells and their potential for immunotherapy. *Int. J. Biol. Sci.* **10**, 119–135 (2014). doi:10.7150/ijbs.7823 Medline
7. J. Zheng, Y. Liu, Y. L. Lau, W. Tu, γδ-T cells: An unpolished sword in human anti-infection immunity. *Cell. Mol. Immunol.* **10**, 50–57 (2013). doi:10.1038/cmi.2012.43 Medline
8. L. Wang, A. Kamath, H. Das, L. Li, J. F. Bukowski, Antibacterial effect of human V gamma 2V delta 2 T cells in vivo. *J. Clin. Invest.* **108**, 1349–1357 (2001). doi:10.1172/JCI200113584 Medline
9. D. I. Godfrey, J. Le Nours, D. M. Andrews, A. P. Uldrich, J. Rossjohn, Unconventional T Cell Targets for Cancer Immunotherapy. *Immunity* **48**, 453–473 (2018). doi:10.1016/j.immuni.2018.03.009 Medline
10. H. Wang, Z. Fang, C. T. Morita, Vgamma2Vdelta2 T Cell Receptor recognition of prenyl pyrophosphates is dependent on all CDRs. *J. Immunol.* **184**, 6209–6222 (2010). doi:10.4049/jimmunol.1000231 Medline
11. C. T. Morita, E. M. Beckman, J. F. Bukowski, Y. Tanaka, H. Band, B. R. Bloom, D. E. Golan, M. B. Brenner, Direct presentation of nonpeptide prenyl pyrophosphate antigens to human gamma delta T cells. *Immunity* **3**, 495–507 (1995). doi:10.1016/1074-7613(95)90178-7 Medline
12. C. Harly, Y. Guillaume, S. Nedellec, C.-M. Peigné, H. Mönkkönen, J. Mönkkönen, J.

Li, J. Kuball, E. J. Adams, S. Netzer, J. Déchanet-Merville, A. Léger, T. Herrmann, R. Breathnach, D. Olive, M. Bonneville, E. Scotet, Key implication of CD277/butyrophilin-3 (BTN3A) in cellular stress sensing by a major human γδ T-cell subset. *Blood* **120**, 2269–2279 (2012). doi:10.1182/blood-2012-05-430470 Medline
13. D. A. Rhodes, H.-C. Chen, A. J. Price, A. H. Keeble, M. S. Davey, L. C. James, M. Eberl, J. Trowsdale, Activation of human γδ T cells by cytosolic interactions of BTN3A1 with soluble phosphoantigens and the cytoskeletal adaptor periplakin. *J. Immunol.* **194**, 2390–2398 (2015). doi:10.4049/jimmunol.1401064 Medline
14. Z. Sebestyen, W. Scheper, A. Vyborova, S. Gu, Z. Rychnavska, M. Schiffler, A. Cleven, C. Chéneau, M. van Noorden, C.-M. Peigné, D. Olive, R. J. Lebbink, R. Oostvogels, T. Mutis, G. J. Schuurhuis, E. J. Adams, E. Scotet, J. Kuball, RhoB Mediates Phosphoantigen Recognition by Vγ9Vδ2 T Cell Receptor. *Cell Reports* **15**, 1973–1985 (2016). doi:10.1016/j.celrep.2016.04.081 Medline
15. S. Gu, J. R. Sachleben, C. T. Boughter, W. I. Nawrocka, M. T. Borowska, J. T. Tarrasch, G. Skiniotis, B. Roux, E. J. Adams, Phosphoantigen-induced conformational change of butyrophilin 3A1 (BTN3A1) and its implication on Vγ9Vδ2 T cell activation. *Proc. Natl. Acad. Sci. U.S.A.* **114**, E7311–E7320 (2017). doi:10.1073/pnas.1707547114 Medline
16. M. Salim, T. J. Knowles, A. T. Baker, M. S. Davey, M. Jeeves, P. Sridhar, J. Wilkie, C. R. Willcox, H. Kadri, T. E. Taher, P. Vantourout, A. Hayday, Y. Mehellou, F. Mohammed, B. E. Willcox, BTN3A1 Discriminates γδ T Cell Phosphoantigens from Nonantigenic Small Molecules via a Conformational Sensor in Its B30.2 Domain. *ACS Chem. Biol.* **12**, 2631–2643 (2017). doi:10.1021/acschembio.7b00694 Medline
17. Y. Yang, L. Li, L. Yuan, X. Zhou, J. Duan, H. Xiao, N. Cai, S. Han, X. Ma, W. Liu, C.-C. Chen, L. Wang, X. Li, J. Chen, N. Kang, J. Chen, Z. Shen, S. R. Malwal, W. Liu, Y. Shi, E. Oldfield, R.-T. Guo, Y. Zhang, A Structural Change in Butyrophilin upon Phosphoantigen Binding Underlies Phosphoantigen-Mediated Vγ9Vδ2 T Cell Activation. *Immunity* **50**, 1043–1053.e5 (2019). doi:10.1016/j.immuni.2019.02.016 Medline
18. L. Starick, F. Riano, M. M. Karunakaran, V. Kunzmann, J. Li, M. Kreiss, S. Amslinger, E. Scotet, D. Olive, G. De Libero, T. Herrmann, Butyrophilin 3A (BTN3A, CD277)-specific antibody 20.1 differentially activates Vγ9Vδ2 TCR clonotypes and interferes with phosphoantigen activation. *Eur. J. Immunol.* **47**, 982–992 (2017). doi:10.1002/eji.201646818 Medline
19. F. Riaño, M. M. Karunakaran, L. Starick, J. Li, C. J. Scholz, V. Kunzmann, D. Olive, S. Amslinger, T. Herrmann, Vγ9Vδ2 TCR-activation by phosphorylated antigens requires butyrophilin 3 A1 (BTN3A1) and additional genes on human chromosome 6. *Eur. J. Immunol.* **44**, 2571–2576 (2014). doi:10.1002/eji.201444712 Medline
20. A. Behren, M. Anaka, P.-H. Lo, L. J. Vella, I. D. Davis, J. Catimel, T. Cardwell, C. Gedye, C. Hudson, R. Stan, J. Cebon, The Ludwig institute for cancer research Melbourne melanoma cell line panel. *Pigment Cell Melanoma Res.* **26**, 597–600 (2013). doi:10.1111/pcmr.12097 Medline
21. G. Malcherek, L. Mayr, P. Roda-Navarro, D. Rhodes, N. Miller, J. Trowsdale, The B7 homolog butyrophilin BTN2A1 is a novel ligand for DC-SIGN. *J. Immunol.* **179**, 3804–3811 (2007). doi:10.4049/jimmunol.179.6.3804 Medline
22. P. Batard, J. Szollosi, I. Luescher, J.-C. Cerottini, R. MacDonald, P. Romero, Use of phycoerythrin and allophycocyanin for fluorescence resonance energy transfer analyzed by flow cytometry: Advantages and limitations. *Cytometry* **48**, 97–105 (2002). doi:10.1002/cyto.10106 Medline
23. M. E. Birnbaum, J. L. Mendoza, D. K. Sethi, S. Dong, J. Glanville, J. Dobbins, E. Özkan, M. M. Davis, K. W. Wucherpfennig, K. C. Garcia, Deconstructing the peptide-MHC specificity of T cell recognition. *Cell* **157**, 1073–1087 (2014). doi:10.1016/j.cell.2014.03.047 Medline
24. A. J. Roelofs, M. Jauhiainen, H. Mönkkönen, M. J. Rogers, J. Mönkkönen, K. Thompson, Peripheral blood monocytes are responsible for gammadelta T cell activation induced by zoledronic acid through accumulation of IPP/DMAPP. *Br. J. Haematol.* **144**, 245–250 (2009). doi:10.1111/j.1365-2141.2008.07435.x Medline
25. T. J. Allison, C. C. Winter, J. J. Fournié, M. Bonneville, D. N. Garboczi, Structure of a human gammadelta T-cell antigen receptor. *Nature* **411**, 820–824 (2001). doi:10.1038/35081115 Medline
26. A. P. Uldrich, J. Le Nours, D. G. Pellicci, N. A. Gherardin, K. G. McPherson, R. T. Lim, O. Patel, T. Beddoe, S. Gras, J. Rossjohn, D. I. Godfrey, CD1d-lipid antigen recognition by the γδ TCR. *Nat. Immunol.* **14**, 1137–1145 (2013). doi:10.1038/ni.2713 Medline
27. P. Vantourout, A. Laing, M. J. Woodward, I. Zlatareva, L. Apolonia, A. W. Jones, A. P. Snijders, M. H. Malim, A. C. Hayday, Heteromeric interactions regulate butyrophilin (BTN) and BTN-like molecules governing γδ T cell biology. *Proc. Natl. Acad. Sci. U.S.A.* **115**, 1039–1044 (2018). doi:10.1073/pnas.1701237115 Medline
28. S. Vavassori, A. Kumar, G. S. Wan, G. S. Ramanjaneyulu, M. Cavallari, S. El Daker, T. Beddoe, A. Theodossis, N. K. Williams, E. Gostick, D. A. Price, D. U. Soudamini, K. K. Voon, M. Olivo, J. Rossjohn, L. Mori, G. De Libero, Butyrophilin 3A1 binds phosphorylated antigens and stimulates human γδ T cells. *Nat. Immunol.* **14**, 908–916 (2013). doi:10.1038/ni.2665 Medline
29. R. Di Marco Barros, N. A. Roberts, R. J. Dart, P. Vantourout, A. Jandke, O. Nussbaumer, L. Deban, S. Cipolat, R. Hart, M. L. Iannitto, A. Laing, B. Spencer-Dene, P. East, D. Gibbons, P. M. Irving, P. Pereira, U. Steinhoff, A. Hayday, Epithelia Use Butyrophilin-like Molecules to Shape Organ-Specific γδ T Cell Compartments. *Cell* **167**, 203–218.e17 (2016). doi:10.1016/j.cell.2016.08.030 Medline
30. D. Melandri, I. Zlatareva, R. A. G. Chaleil, R. J. Dart, A. Chancellor, O. Nussbaumer, O. Polyakova, N. A. Roberts, D. Wesch, D. Kabelitz, P. M. Irving, S. John, S. Mansour, P. A. Bates, P. Vantourout, A. C. Hayday, The γδTCR combines innate immunity with adaptive immunity by utilizing spatially distinct regions for agonist selection and antigen responsiveness. *Nat. Immunol.* **19**, 1352–1365 (2018). doi:10.1038/s41590-018-0253-5 Medline
31. B. Castella, J. Kopecka, P. Sciancalepore, G. Mandili, M. Foglietta, N. Mitro, D. Caruso, F. Novelli, C. Riganti, M. Massaia, The ATP-binding cassette transporter A1 regulates phosphoantigen release and Vγ9Vδ2 T cell activation by dendritic cells. *Nat. Commun.* **8**, 15663 (2017). doi:10.1038/ncomms15663 Medline
32. J. Holst, A. L. Szymczak-Workman, K. M. Vignali, A. R. Burton, C. J. Workman, D. A. A. Vignali, Generation of T-cell receptor retrogenic mice. *Nat. Protoc.* **1**, 406–417 (2006). doi:10.1038/nprot.2006.61 Medline
33. J. Joung, S. Konermann, J. S. Gootenberg, O. O. Abudayyeh, R. J. Platt, M. D. Brigham, N. E. Sanjana, F. Zhang, Genome-scale CRISPR-Cas9 knockout and transcriptional activation screening. *Nat. Protoc.* **12**, 828–863 (2017). doi:10.1038/nprot.2017.016 Medline
34. S. Chen, N. E. Sanjana, K. Zheng, O. Shalem, K. Lee, X. Shi, D. A. Scott, J. Song, J. Q. Pan, R. Weissleder, H. Lee, F. Zhang, P. A. Sharp, Genome-wide CRISPR screen in a mouse model of tumor growth and metastasis. *Cell* **160**, 1246–1260 (2015). doi:10.1016/j.cell.2015.02.038 Medline
35. M. Martin, Cutadapt removes adapter sequences from high-throughput sequencing reads. *EMBnet J.* **17**, 10–12 (2011). doi:10.14806/ej.17.1.200
36. M. D. Robinson, D. J. McCarthy, G. K. Smyth, edgeR: A Bioconductor package for differential expression analysis of digital gene expression data. *Bioinformatics* **26**, 139–140 (2010). doi:10.1093/bioinformatics/btp616 Medline
37. A. R. Aricescu, W. Lu, E. Y. Jones, A time- and cost-efficient system for high-level protein production in mammalian cells. *Acta Crystallogr. D Biol. Crystallogr.* **62**, 1243–1250 (2006). doi:10.1107/S0907444906029799 Medline
38. H. F. Koay, N. A. Gherardin, C. Xu, R. Seneviratna, Z. Zhao, Z. Chen, D. P. Fairlie, J. McCluskey, D. G. Pellicci, A. P. Uldrich, D. I. Godfrey, Diverse MR1-restricted T cells in mice and humans. *Nat. Commun.* **10**, 2243 (2019). doi:10.1038/s41467-019-10198-w Medline

ACKNOWLEDGMENTS

We thank Z. Chen and L. Kjer-Nielsen for kindly providing parental J.RT3-T3.5 cells, and P. Neeson for kindly providing zoledronic acid. The authors thank Z. Tian for technical assistance. We also thank T. Luke and staff at the Doherty Institute Flow Cytometry Facility, V. Jameson and staff at the Melbourne Brain Centre Flow Cytometry Facility, A. Gonzalez from the Melbourne Cytometry Platform, and D. Baloyan at the Olivia Newton-John Cancer Research Institute for flow cytometry support. We thank P. McMillan and staff at the Biological Optical Microscopy Platform for microscopy support. We thank staff at AGRF for DNA sequencing support, and Y. Mok from the Melbourne Protein Characterisation Platform for ITC support. **Funding:** This work was supported by the Cancer Council of Victoria (#1126866), the Australian Research Council (ARC; CE140100011, DP170102471), the National Health and Medical Research Council of Australia (NHMRC; 1165467, 1113293), and the Operational Infrastructure Support Program provided by the Victorian Government, Australia. APU was

supported by an ARC Future Fellowship (FT140100278); AB is supported by a fellowship from the Department of Health and Human Services acting through the Victorian Cancer Agency; DIG is supported by an NHMRC Senior Principal Research Fellowship (1117766); MR is supported by the Deutsche Forschungsgemeinschaft (GRK2168) and the University of Melbourne through the International Research and Research Training Fund; JAV is supported by an NHMRC Principal Research Fellowship (1154502); HEGM is supported by an ARC Discovery Early Career Researcher Award (DE170100575) and the AMP Tomorrow Fund. **Author contributions:** Conceptualization, APU, AB, DIG, JC; methodology, APU, AB, DG, MR, SO; investigation, MR, SO, TSF, DJ, AB, APU; resources, KW, ZR, HEGM, CH, CT, AKW, SJK, JAV, BP, JS, MP, ADN, AH, AMV, GV, EM, CP, NAG, JC, DIG, AB, APU; writing – original draft, APU, AB, DIG, MR; writing – reviewing and editing, APU, AB, DIG, MR, TSF, DNJ, HEGM, SJK, NAG; supervision, APU, AB, DIG, JC, NAG, CK; funding acquisition, APU, AB, DIG. **Competing interests:** ADN, JS, MP, AH, AMV, GV, EM and CP are employees of CSL Limited and are able to partake in employee share schemes. Some of the authors including MR, SO, TF, CH, KW, AH, AMV, EM, CP, JC, DIG, AB, and APU are listed as inventors on patent applications related to the use of BTN2A1 to influence immune reactions. AB and JC received research funding from CSL Limited. All other authors declare no competing interests. **Data and materials availability:** Raw data and analysis scripts associated with the whole-genome screen depicted in Fig. 1B are available in database S1. Anti-BTN Abs are available from GV at CSL Limited upon request. All data necessary to understand and evaluate the conclusions of this paper are provided in the manuscript and supplementary materials.

SUPPLEMENTARY MATERIALS

science.sciencemag.org/cgi/content/full/science.aay5516/DC1
Figs. S1 to S17
Tables S1 and S2
Database S1

28 June 2019; resubmitted 14 October 2019
Accepted 23 December 2019
Published online 9 January 2020
10.1126/science.aay5516

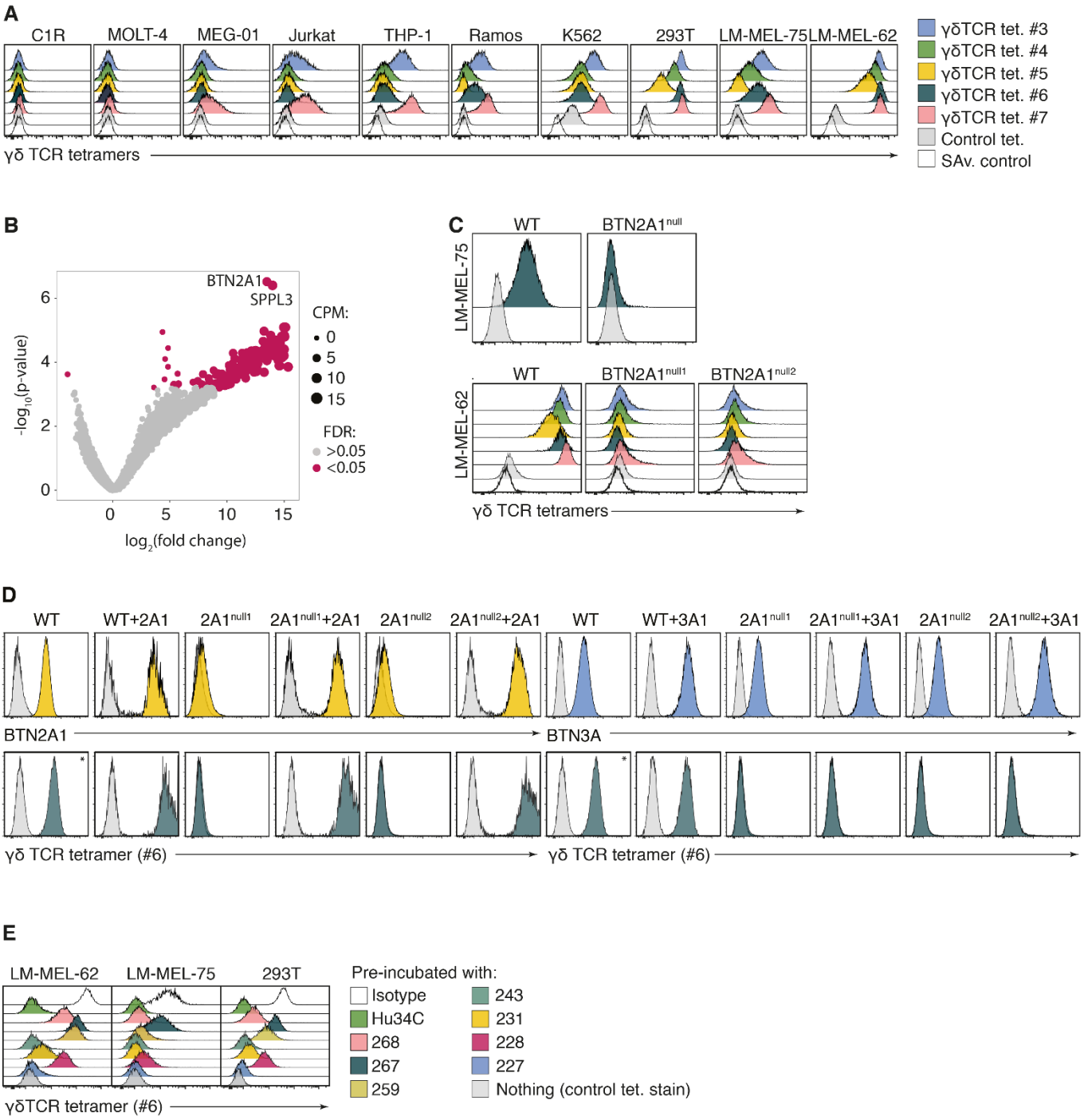

Fig. 1. Vγ9Vδ2⁺ γδ T cell receptor tetramer staining is dependent on BTN2A1. (**A**) Vγ9Vδ2⁺ γδTCR tetramer staining of various cell lines. Colored histograms depict γδTCR tetramers #3–#7; gray, irrelevant control (mouse CD1d–α-GalCer) tetramer; white, streptavidin (SAv)-PE control. (**B**) Volcano plot depicting $\log_2$ (fold-change) versus $-\log_{10}$ (p-value) for each gRNA, between unsorted and Vγ9Vδ2 γδTCR tetramer^{lo} LM-MEL-62 cells, where magenta depicts significant differences (false discovery rate (FDR) < 0.05). CPM, counts per million. (**C**) Vγ9Vδ2⁺ γδTCR tetramer staining of LM-MEL-62 *BTN2A1*^{null} and LM-MEL-75 *BTN2A1*^{null} cells compared to parental cells. Color scheme as in (A). (**D**) Anti-BTN2A1 mAb (clone 231, yellow), anti-BTN3A1/3A2/3A3 mAb (clone 103.2, blue), and Vγ9Vδ2⁺ γδTCR tetramer (#6) staining (dark green) on parental and *BTN2A1*$^{null1/null2}$ LM-MEL-62 cells transfected with either *BTN2A1* or *BTN3A1*. *γδTCR tetramer staining is depicted twice. (**E**) Vγ9Vδ2⁺ γδTCR tetramer #6 staining of LM-MEL-62, LM-MEL-75, and HEK-293T cells, following pre-incubation of cells with a panel of anti-BTN2A1 mAb (colored histograms), compared to isotype control (white). Lower histograms (gray) depict control staining with irrelevant mouse CD1d–α-GalCer tetramer. tet, tetramer. Data in (A), (C), (D), and (E) are representative of two independent experiments.

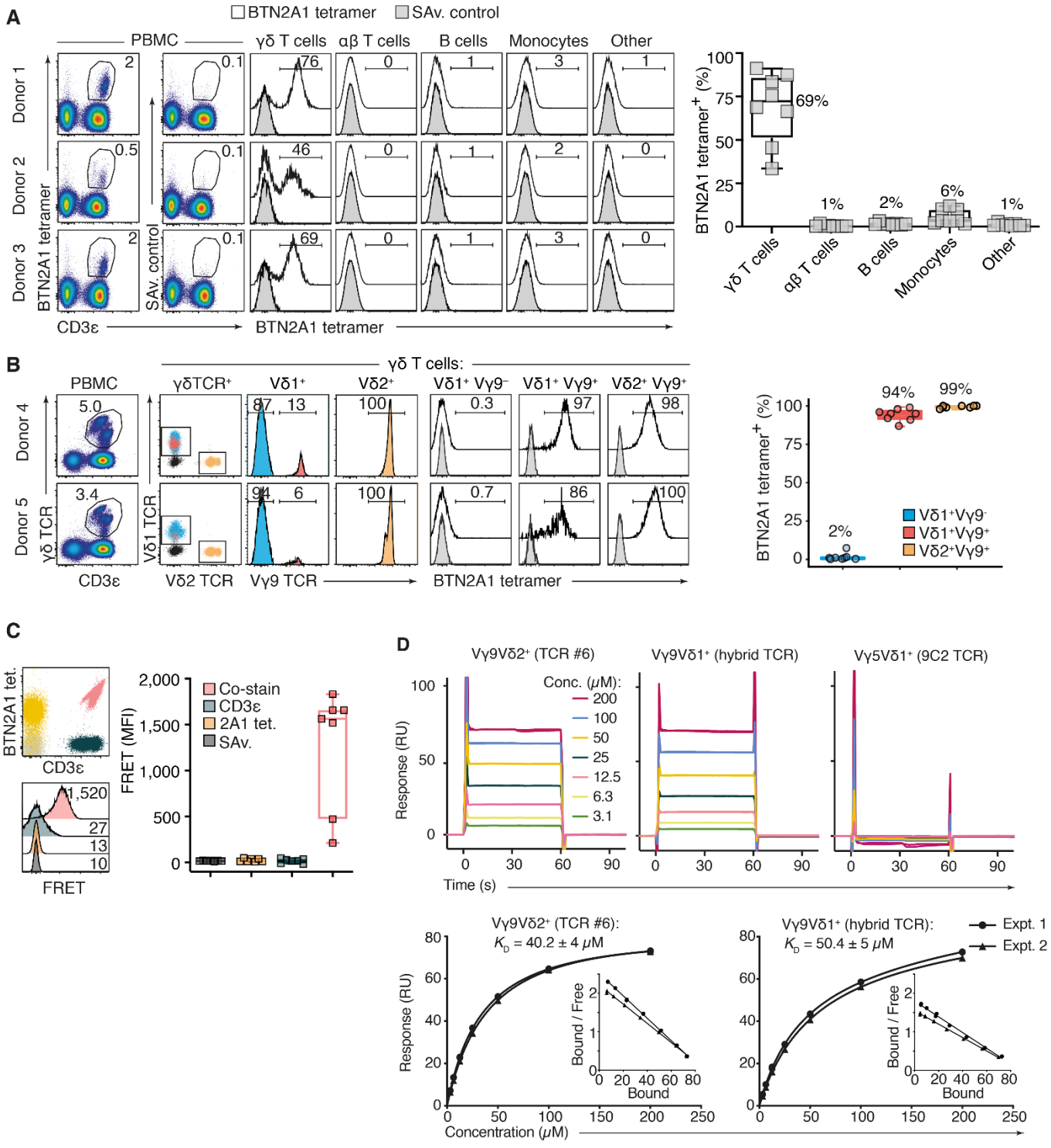

Fig. 2. BTN2A1 binds $V_\gamma9^+$ γδ T cell receptors. (**A**) BTN2A1 tetramer-PE (first column) or streptavidin-PE control (second column) versus CD3ε staining on three representative human PBMC samples. Histograms depict BTN2A1 tetramer-PE staining (white) or streptavidin-PE control (gray) on gated γδ T cell ($CD3^+\gamma\delta TCR^+$), αβ T cell ($CD3^+\gamma\delta TCR^-$), B cell ($CD3^-CD19^+$), monocyte ($CD3^-CD19^-CD14^+$) or other ($CD3^-CD19^-CD14^-$) subsets. Box-and-whisker plots (right) depict the percentage of each cell lineage that binds to BTN2A1 tetramer in blood samples from different donors. (**B**) BTN2A1 tetramer (white histograms) overlaid with streptavidin-PE alone control (gray histograms) staining, on $V_\gamma9^+V\delta2^+$ (orange), $V_\gamma9^+V\delta1^+$ (red), or $V_\gamma9^-V\delta1^+$ (blue) T cells, with parent gating shown to the left. Box-and-whisker plots (right) depict the percentage of each γδ T cell subset that binds to BTN2A1 tetramer-PE in different donors. (**C**) FRET fluorescence (histogram overlays) between BTN2A1 tetramer-PE and CD3ε-APC on dual-stained (pink) or single-stained controls (orange and dark green, respectively), using purified in vitro-expanded $V\delta2^+$ T cells. Box-and-whisker plots depict FRET mean fluorescence intensity (MFI) in γδ T cell subsets from different human donors. (**D**) Binding of soluble BTN2A1 (200–3.1 μM) to immobilized $V_\gamma9^+V\delta2^+$ ('TCR #6', left), $V_\gamma9^+V\delta1^+$ ('hybrid', middle) and $V_\gamma5^+V\delta1^+$ ('9C2', right) γδTCRs, as measured by surface plasmon resonance. Saturation plots (below) depict binding at equilibrium, and Scatchard plots. K_D, dissociation constant at equilibrium ± SEM; SAv, streptavidin. Data in (A) represent n=8 donors pooled from two independent experiments; (B) n=8 donors from two experiments; (C) n=7 donors pooled from three independent experiments; (D) n=2 separate experiments, one of which (Expt 2) was performed in duplicate and averaged.

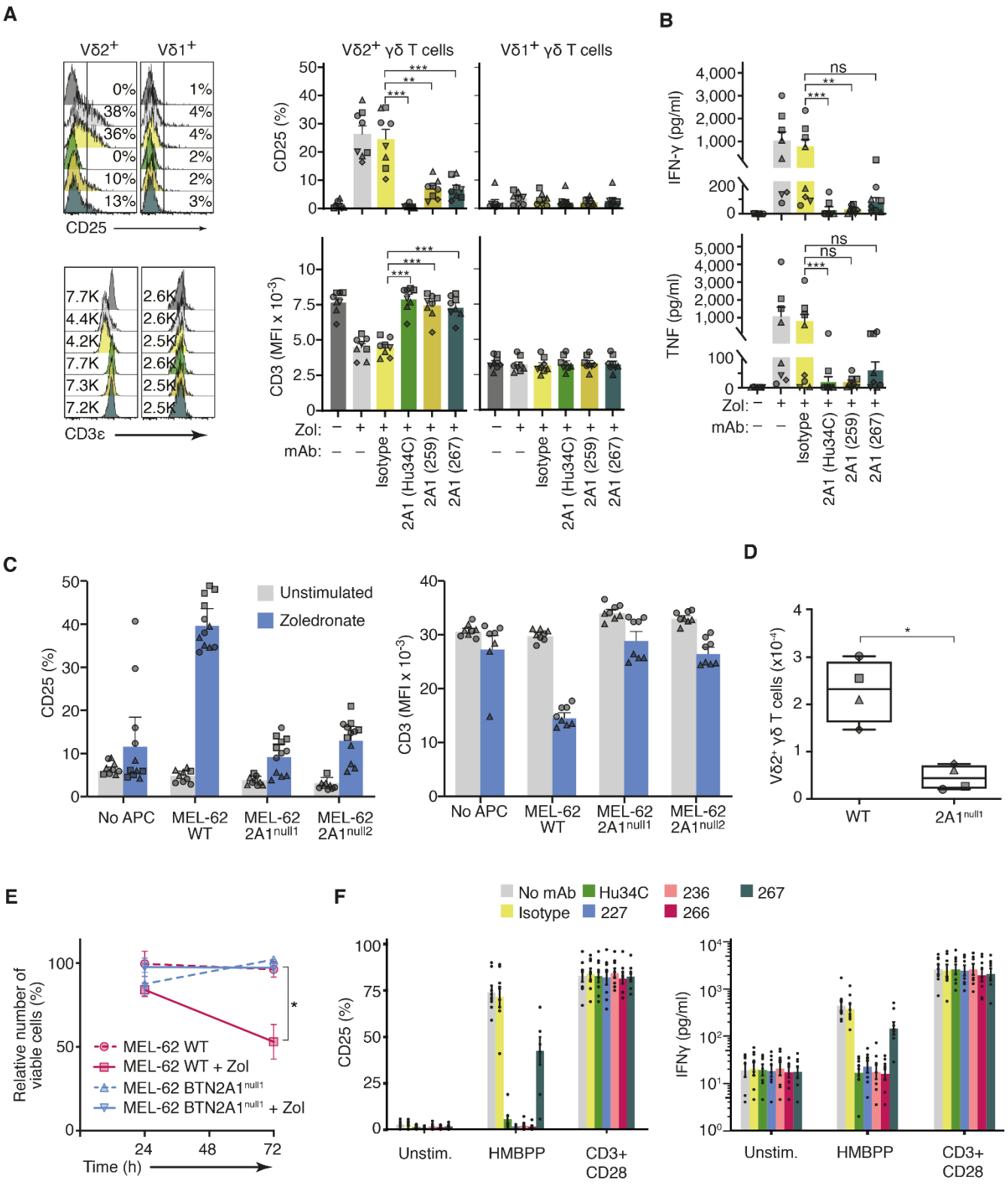

Fig. 3. γδ T cell functional responses to pAg depend on BTN2A1. (**A**) CD25 expression and CD3ε mean fluorescence intensity (MFI) on Vδ2$^+$ and control Vδ1$^+$ T cells gated among PBMCs cultured for 24 hours ± 4 μM zoledronate and ± 10 μg/ml neutralizing anti-BTN2A1 mAb as indicated. *, p<0.05; **, p<0.01, ***, p<0.001, by ANOVA. (**B**) IFN-γ and TNF concentration in the culture supernatants from (A). **, p<0.01; ***, p<0.001, by Friedman test. (**C**) CD3 MFI and CD25 expression on purified in vitro-expanded Vδ2$^+$ T cells co-cultured with parental or *BTN2A1*^{null} LM-MEL-62 APCs without (gray) or with (blue) 4 μM zoledronate. Each symbol represents a different donor. Bar graphs depict mean ± SEM. (**D**) Number of Vδ2$^+$ γδ T cells in co-cultures of PBMC with parental or *BTN2A1*^{null1} LM-MEL-62 APC after a 2-day challenge with 1 μM zoledronate followed by maintenance of non-adherent PBMCs for an additional 7 days in media containing IL-2. *, p<0.05 using a Mann–Whitney test. (**E**) Cell viability (mean ± SEM) as determined using the metabolic dye MTS, normalized against input cell number, of co-cultures of parental (WT) or BTN2A1^{null} LM-MEL-62 targets with in vitro-expanded Vδ2$^+$ T cells, at the indicated time points ± 1 μM zoledronate. *, p<0.05 using a Mann–Whitney test between zoledronate-treated groups. (**F**) CD25 expression (left) and IFN-γ concentration (right) following culture of purified in vitro-expanded Vδ2$^+$ T cells with HMBPP (0.5 ng/ml) or plate-bound anti-CD3 plus anti-CD28 (10 μg/ml each) ± 10 μg/ml neutralizing anti-BTN2A1 mAb. Data in (A) and (B) n=8 donors pooled from two independent experiments; (C) n=3 donors pooled from three independent experiments, each performed with n=4 technical replicates indicated by different symbols; (D) n=4 donors, each averaged from 1–5 technical replicates across five independent experiments; (E) n=8 donors pooled from two independent experiments; (F) n=4 donors, each averaged from 2–6 technical replicates across six independent experiments. Zol, zoledronate.

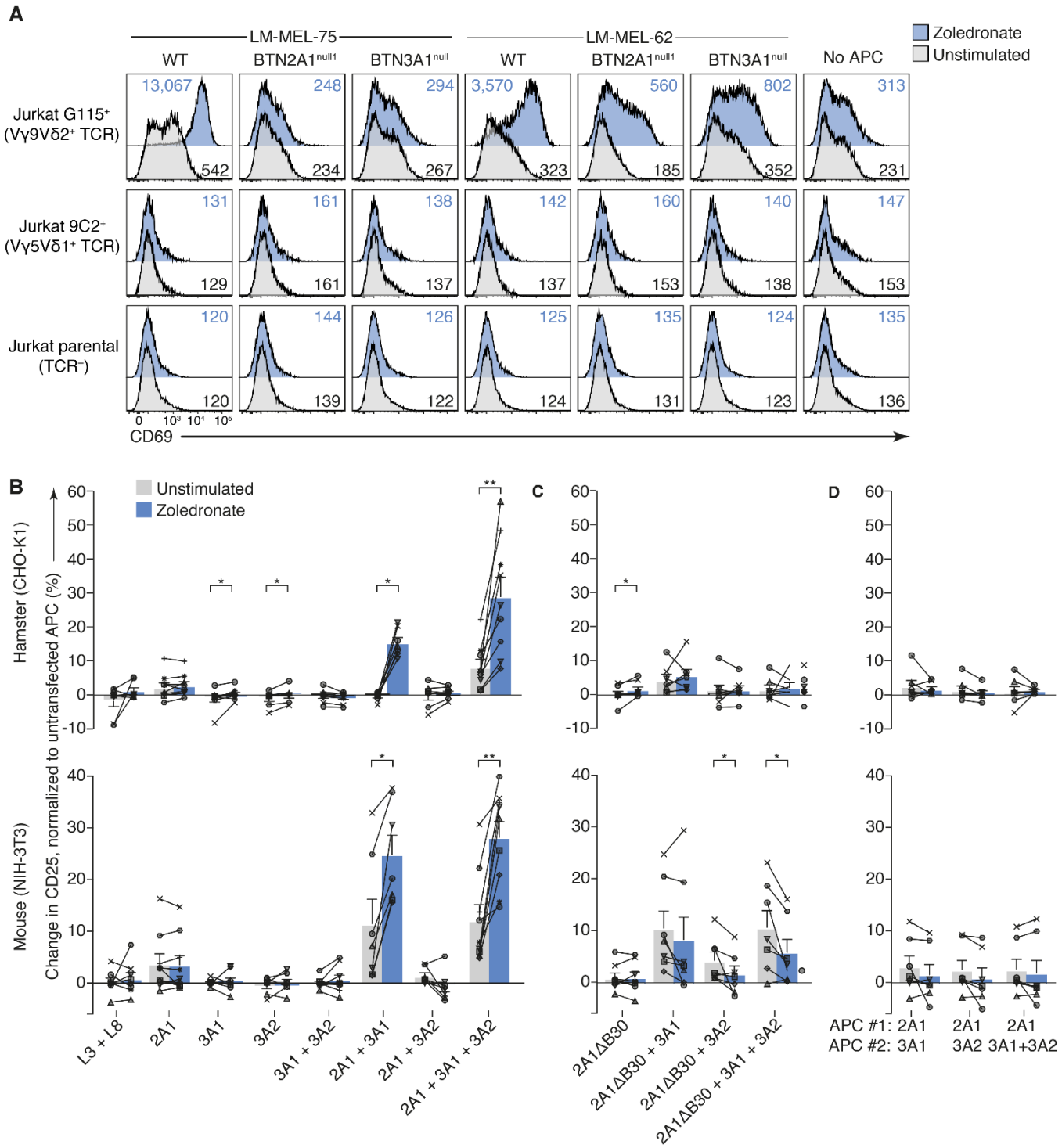

Fig. 4. BTN2A1 and BTN3A1 are both necessary for pAg presentation. (**A**) CD69 expression on G115 $V_\gamma 9V\delta 2^+$ $\gamma\delta$TCR (top row), 9C2 $V_\gamma 5V\delta 1^+$ $\gamma\delta$ TCR (middle), and parental (TCR^-) J.RT3-T3.5 (bottom row) Jurkat cells after overnight co-culture with the indicated APCs, in the presence (blue) or absence (gray) of 40 μM zoledronate. Numbers indicate the median fluorescence intensity. (**B**) Change in CD25 expression (normalized to unstimulated control for each sample) on purified in vitro-expanded $\gamma\delta$ T cells co-cultured for 24 hours in the presence (blue) or absence (gray) of 4 μM zoledronate with CHO-K1 (hamster origin) or NIH-3T3 (mouse origin) APCs transfected with the indicated combinations of (B) *BTNL3*, *BTNL8*, *BTN2A1*, *BTN3A1*, and *BTN3A2*, or (**C**) *BTN2A1ΔB30*, *BTN3A1*, and *BTN3A2*. (**D**) $\gamma\delta$ T cells co-cultured as in (A), except in the presence of a 1:1 mixture of two populations of APCs, each transfected separately with combinations of *BTN2A1*, *BTN3A1*, and *BTN3A2*. Each symbol and connecting line represents a different donor. *, $p < 0.05$; **, $p < 0.01$ using a Wilcoxon paired test. Bar graphs depict mean ± SEM. Data in (A) representative of one of three similar experiments; (B-D) represents n=7–9 donors per group pooled from 3–5 independent experiments.

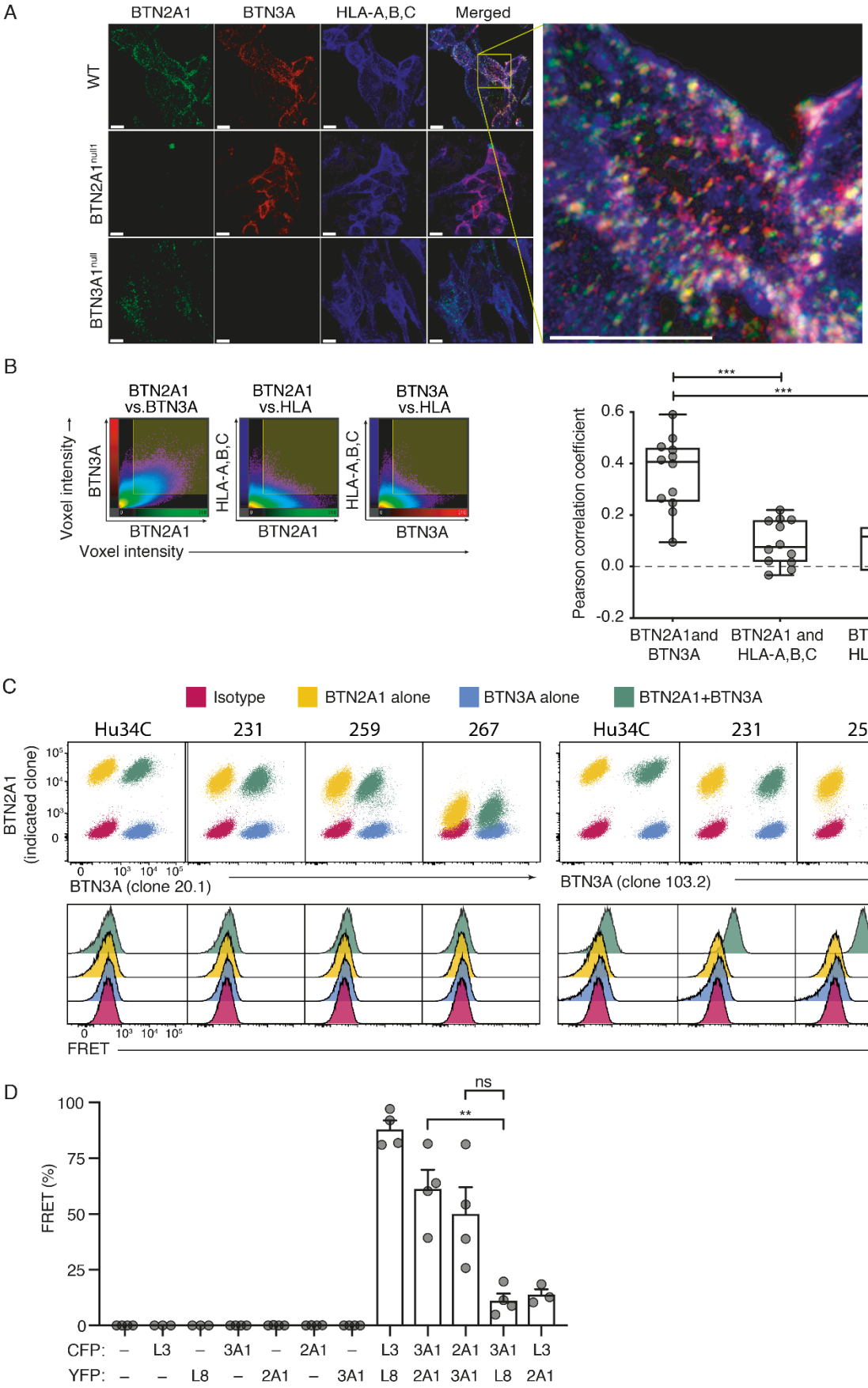

Fig. 5. BTN2A1 associates with BTN3A1 on the cell surface. (**A**) Z-stack confocal microscopy of surface BTN2A1 (green, clone 259), BTN3A (red, clone 103.2), and pan-HLA class I (blue, clone W6/32) on parental LM-MEL-75 ("WT", top row), *BTN2A1*^{null} (middle row) and *BTN3A1*^{null} (bottom row) cells. Scale bars = 10 μm. (**B**) Graph depicts Pearson correlation coefficients for individual fields of view. Representative voxel density plots depicting correlation between anti-BTN2A1 versus anti-BTN3A1/3A2/3A3 ("BTN3A") (left), anti-BTN2A1 versus anti- HLA-A,B,C (middle), and anti-BTN3A versus anti-HLA-A,B,C (right). ***, $p<0.001$ using a Kruskal–Wallis with Dunn's post-test. (**C**) Anti-BTN2A1 versus BTN3A co-staining (green), or single staining (yellow and blue, respectively), or mouse IgG1 versus mouse IgG2a isotype control staining (*x*- and *y*-axis respectively, magenta) on LM-MEL-75 cells using the indicated mAb clones (top row). Histograms (second row) depict FRET fluorescence. (**D**) Percentage of FRET^{+} cells between butyrophilin$^{CFP/YFP}$-transfected NIH-3T3 cells. Data are representative of (A) and (B) two pooled independent experiments; (C) one experiment; (D) four independent experiments.

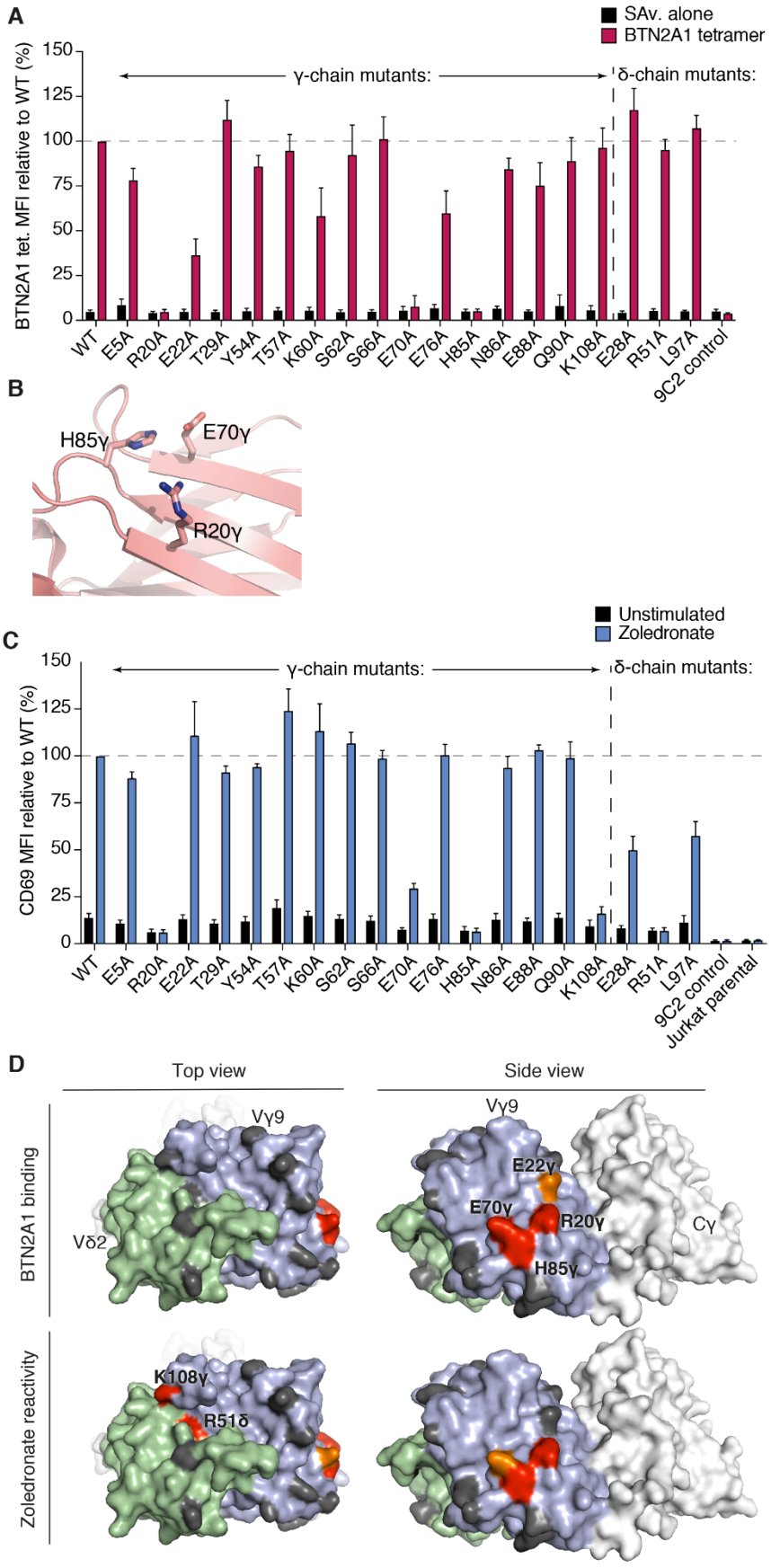

Fig. 6. Vγ9Vδ2⁺ γδ T cell receptors contain two distinct ligand-binding domains. (**A**) BTN2A1 tetramer-PE (red) and control streptavidin-PE alone (black) staining of gated GFP⁺CD3⁺ HEK-293T cells transfected with single-residue G115 γδTCR alanine mutants (or control Jurkat 9C2 γδTCR), normalized to BTN2A1 tetramer staining of G115 WT γδTCR. (**B**) Cartoon view of the G115 γδTCR (pdb code 1HXM (*25*)) Vγ9 ABED β-sheet depicting the side chains of R20, E70, and H85. (**C**) CD69 expression on Jurkat cells expressing G115 γδTCR alanine mutants (or 9C2 γδTCR⁺ or parental γδTCR⁻ Jurkat cells), normalized to the activation levels of G115 WT γδTCR⁺ Jurkat cells, after overnight culture with LM-MEL-75 APCs in the presence (blue) or absence (black) of 40 μM zoledronate. (**D**) Surface of G115 γδTCR (pdb code 1HXM (*25*)) depicting the residues important for BTN2A1 tetramer binding (top row) and zoledronate reactivity (bottom row). Side chains of residues with >75% loss of BTN2A1 binding or CD69 induction shown in red; 50%–75% reduction in orange; <50% reduction in gray; Vδ2, green; Vγ9, blue; constant regions, white. MFI, median fluorescence intensity; SAv, streptavidin alone control; unstim, unstimulated control. Data in (A) and (B) represent the mean ± SEM of N=3 separate experiments.

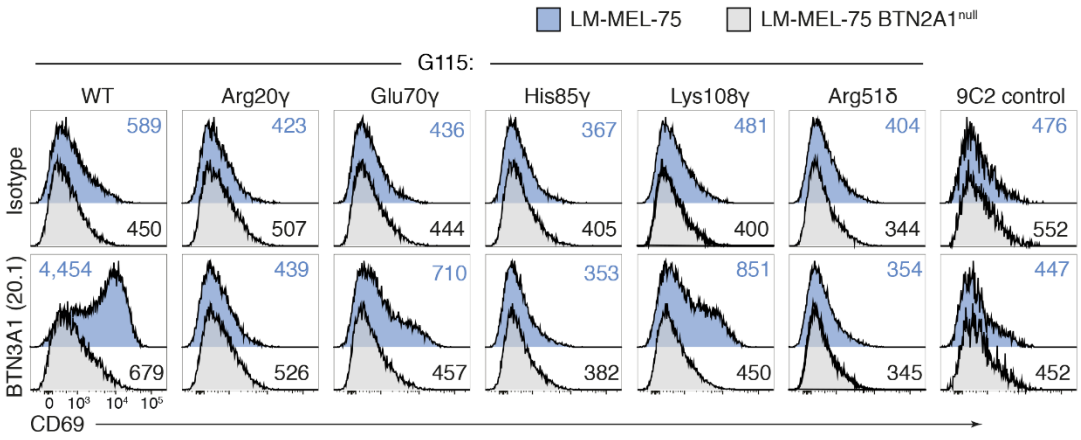

Fig. 7. Agonistic activity of anti-BTN3A1 mAb clone 20.1 depends on BTN2A1. CD69 expression on Jurkat cells expressing $V_\gamma 9V\delta 2^+$ γδTCR (clone G115), or the indicated G115 γδTCR mutants, or control $V_\gamma 5V\delta 1^+$ γδTCR (clone 9C2) following co-culture with either parental LM-MEL-75 ("WT") or *BTN2A1*^{null} APCs pre-incubated with anti-BTN3A (clone 20.1, 10 μg/ml, blue histograms) or isotype control (mouse IgG1, 10 μg/ml, gray). Data representative of one of two separate experiments.

Science

Butyrophilin 2A1 is essential for phosphoantigen reactivity by γδ T cells

Marc Rigau, Simone Ostrouska, Thomas S. Fulford, Darryl N. Johnson, Katherine Woods, Zheng Ruan, Hamish E.G. McWilliam, Christopher Hudson, Candani Tutuka, Adam K. Wheatley, Stephen J. Kent, Jose A. Villadangos, Bhupinder Pal, Christian Kurts, Jason Simmonds, Matthias Pelzing, Andrew D. Nash, Andrew Hammet, Anne M. Verhagen, Gino Vairo, Eugene Maraskovsky, Con Panousis, Nicholas A. Gherardin, Jonathan Cebon, Dale I. Godfrey, Andreas Behren and Adam P. Uldrich

published online January 9, 2020

Science (print ISSN 0036-8075; online ISSN 1095-9203) is published by the American Association for the Advancement of Science, 1200 New York Avenue NW, Washington, DC 20005. The title *Science* is a registered trademark of AAAS.